AGU PUBLICATIONS

Paleoceanography

RESEARCH ARTICLE
10.1002/2015PA002922

Key Points:
- Recurrent facies stacking patterns are observed in upper Albian-early Turonian pelagic sequences
- Coupled surface and bottom processes influenced onset and termination of intermittent and prolonged anoxia
- Climate changes were associated with salinity-driven bottom currents redistributing and eroding sediments

Supporting Information:
- Figure S1
- Figure S2
- Figure S3
- Figure S4
- Figure S5
- Figure S6
- Figure S7

Correspondence to:
G. Gambacorta,
gabriele.gambacorta@guest.unimi.it

Citation:
Gambacorta, G., R. Bersezio, H. Weissert, and E. Erba (2016), Onset and demise of Cretaceous oceanic anoxic events: The coupling of surface and bottom oceanic processes in two pelagic basins of the western Tethys, *Paleoceanography*, *31*, 732–757, doi:10.1002/2015PA002922.

Received 23 DEC 2015
Accepted 20 MAY 2016
Accepted article online 23 MAY 2016
Published online 20 JUN 2016

Onset and demise of Cretaceous oceanic anoxic events: The coupling of surface and bottom oceanic processes in two pelagic basins of the western Tethys

G. Gambacorta[1], R. Bersezio[1,2], H. Weissert[3], and E. Erba[1]

[1]Dipartimento di Scienze della Terra "A. Desio", Universita' di Milano, Milan, Italy, [2]CNR-IDPA, Milan, Italy, [3]Geologisches Institut, ETH Zurich, Zürich, Switzerland

Abstract The upper Albian–lower Turonian pelagic successions of the Tethys record processes acting during the onset, core, and recovery from perturbed conditions across oceanic anoxic event (OAE) 1d, OAE 2, and the mid-Cenomanian event I (MCE I) relative to intervening intervals. Five sections from Umbria-Marche and Belluno Basins (Italy) were analyzed at high resolution to assess processes in surface and deep waters. Recurrent facies stacking patterns (SP) and their associations record periods of bottom current activity coupled with surface changes in trophic level. Climate changes appear to have been influential on deep circulation dynamics. Under greenhouse conditions, vigorous bottom currents were arguably induced by warm and dense saline deep waters originated on tropical shelves in the Tethys and/or proto-Atlantic Ocean. Tractive facies postdating intermittent anoxia during OAE 1d and in the interval bracketed by MCE I and OAE 2 are indicative of feeble bottom currents, though capable of disrupting stratification and replenish deep water with oxygen. The major warming at the onset of OAE 2 might have enhanced the formation of warm salty waters, possibly producing local hiatuses at the base of the Bonarelli Level and winnowing at the seafloor. Hiatuses detected at the top of the Bonarelli Level possibly resulted from most effective bottom currents during the early Turonian thermal maximum. Times of minimal sediment displacement correlate with cooler climatic conditions and testify a different mechanism of deep water formation, as further suggested by a color change to reddish lithologies of the post-OAE 1d and post-OAE 2 intervals.

1. Introduction

An enormous amount of literature ranging from sedimentology [*Hsü and Jenkyns*, 1974; *Hüneke and Mulder*, 2011], inorganic/organic and isotopic geochemistry [*Scholle and Arthur*, 1980; *Weissert et al.,* 1985; *Brumsack*, 2006; *Jenkyns*, 2010 with references; *Sinnighe-Damsté et al.,* 2010], and micropaleontology [e.g., *Premoli Silva et al.,* 1999; *Erba*, 2004; *Friedrich et al.,* 2009] describes the oceanic anoxic events (s) in Mesozoic pelagic successions ([*Schlanger and Jenkyns*, 1976]; see *Jenkyns* [2010] for a synthesis). While reconstruction of changes in surface-water paleotemperature, fertility, and chemistry of Cretaceous oceans are widely studied, sea bottom physical processes (sediment deposition and redistribution) and their links to oceanography and climate are still poorly investigated.

In spite of their uniform appearance, pelagic successions include a wide and complex array of facies associations, substantially deriving from surface and bottom water processes. In this paper we investigate the relationship between the importance of surface ocean dynamics and bottom water physicochemical conditions in the vertical facies associations of pelagic successions (stacking patterns—SP). SP should document the succession of processes during the onset, development, and recovery from oceanographic perturbations and in response to these changes.

We focus on the late Albian–early Turonian time interval testifying a supraregional facies change in the Tethys Ocean from varicolored marly lithotypes to whitest limestones [see *Giorgioni et al.*, 2015], which presumably results from a major shift in oceanographic conditions. Moreover, the chosen time window was punctuated by major carbon cycle perturbations, as testified by three positive excursions in $\delta^{13}C$ record [*Jarvis et al.,* 2006; *Jenkyns*, 2010]: oceanic anoxic event (OAE) 1d [*Arthur et al.,* 1990; *Wilson and Norris*, 2001], represented by the uppermost Albian Pialli Level—or Breistoffer Event; the middle Cenomanian event I (MCE I) [*Coccioni and Galeotti*, 2001, 2003] and the OAE 2 [*Schlanger and Jenkyns*, 1976; *Arthur et al.,* 1990], with its sedimentary expression represented in the Italian central Apennines by the bituminous radiolarian-rich Bonarelli Level [*Bonarelli*, 1891].

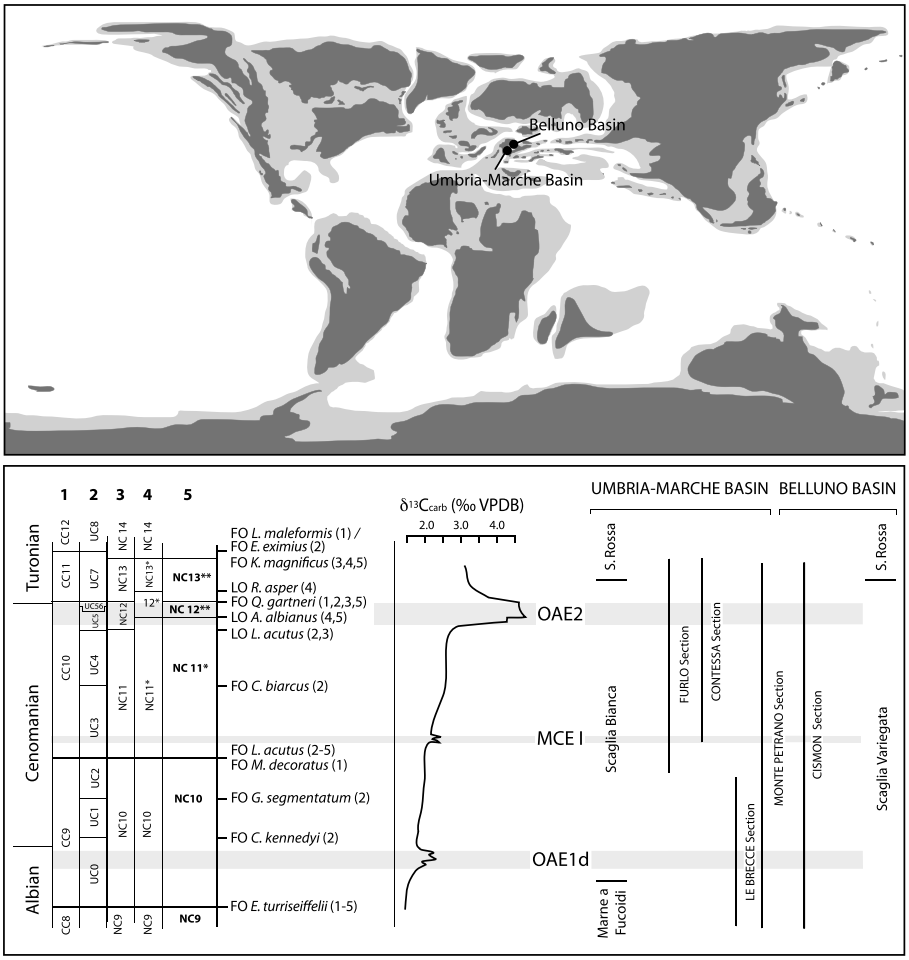

Figure 1. (top) Paleogeographic position of the studied basins during the Cenomanian; emerged lands in dark grey, shallow seas in light grey, deep seas in white (upper sketch; reconstruction based on R.C. Blakey, NAU Geology (http://jan.ucc.nau.edu/~rcb7/90moll.jpg). (bottom) Stratigraphic range of analyzed sections plotted against nannofossil biostratigraphy and chemostratigraphy of the late Albian–early Turonian time interval. Nannofossil zones after 1: *Sissingh* [1977], 2: *Burnett* [1998], 3: *Roth* [1978], 4: *Bralower et al.* [1995], and 5: *Tsikos et al.* [2004]. Carbon isotope curve is a smoothed (5 pt moving average) composite from the English Chalk [*Jarvis et al.,* 2006]. FO: first occurrence and LO: last occurrence (after *Gambacorta et al.* [2015]). Full names of nannofossil species are as follows: *Lucianorhabdus maleformis*, *Eiffellithus eximius, Kamptnerius magnificus, Rhagodiscus asper, Quadrum gartneri, Axopodorhabdus albianus, Lithraphidites acutus, Cylindralithus biarcus, Microrhabdulus decoratus, Gartnerago segmentatum, Corollithion kennedyi*, and *Eiffellithus turriseiffelii*.

The specific purpose of this work is to trace ocean dynamics related to changes in climate and global carbon cycling in pelagic settings during the late Albian–early Turonian interval in the Tethys Ocean. We will test the hypothesis that sedimentary facies associations preserved in pelagic successions record coupled changes in surface and bottom water conditions during the onset and vanishing stages of intermittent basinal dysoxia-anoxia and global oxygen depletion.

During the Mid-Cretaceous, the Tethys Ocean was large and crucially positioned relative to the Indo-Pacific Ocean, while the Atlantic Ocean, widely studied (i.e., recently from *Trabucho-Alexandre et al.* [2010]), was in its early evolutionary phase. Conversely, in absence of continuous and complete records from the Indian and Pacific Oceans, characterization and understanding of physical, chemical, and biological changes and their rates as archived in Tethyan pelagic successions are pivotal for the comprehension of ocean dynamics during times of high CO_2 and greenhouse conditions. The objectives of our study are as follows: (i) to relate the stacking patterns to their high-resolution biochemostratigraphic framework at present available [*Gambacorta et al.,* 2015]; (ii) to understand deep sea dynamics, identifying the eventual occurrence of sediment redistribution processes by bottom currents; (iii) to estimate the coupling or decoupling of surface and

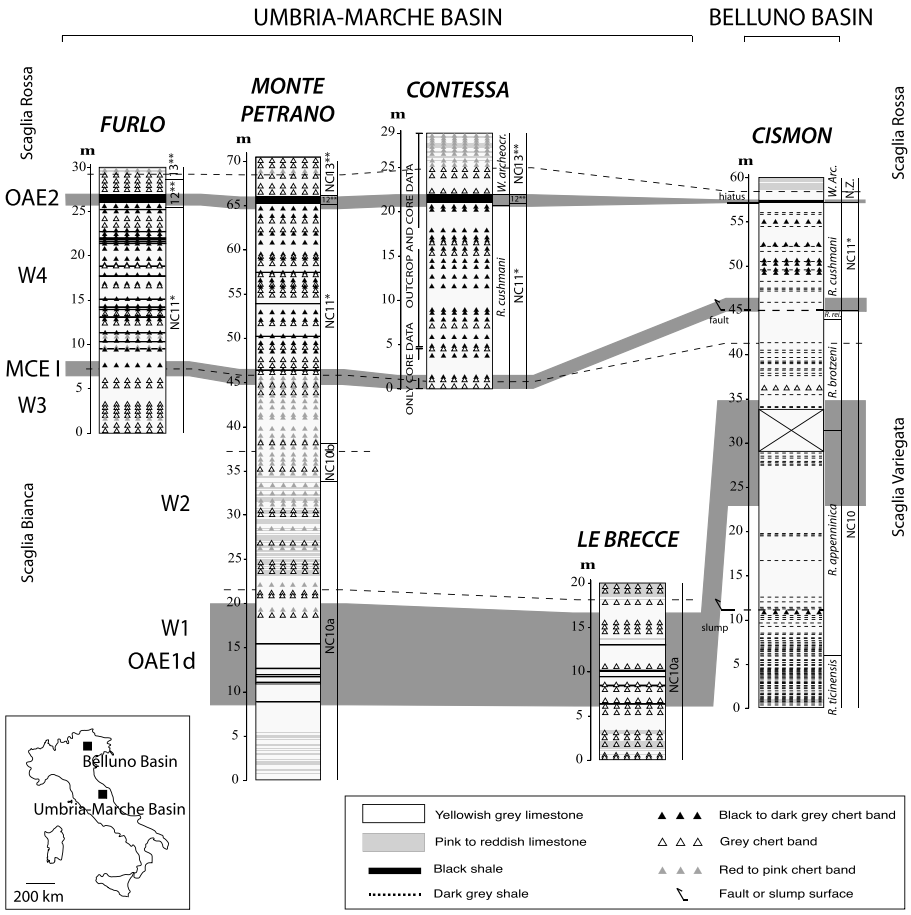

Figure 2. Location of the studied sections. Schematic lithostratigraphy and stratigraphic position of the studied sections (modified after *Gambacorta et al.* [2014]). Grey bands correspond to carbon isotopic anomalies, nannofossil, and planktonic foraminiferal biostratigraphy (as available) are indicated next to each section [*Gambacorta et al.,* 2015].

bottom water changes across and in between times of major perturbations of the C cycle; (iv) to compare the transient intermittent and local pulses of dysoxia/anoxia to the phases of global perturbations. In particular, we want to test the following hypotheses: (1) are facies associations repetitive?; (2) do sedimentation patterns recur at different time scales?; (3) are surface and bottom processes coupled in affecting sedimentation patterns and who predominates?; (4) are onset and termination of anoxic conditions linked to specific types of surface-water changes and/or bottom water currents?; (5) what is the influence of bottom current activity on oxygen distribution at the seafloor and anoxia termination?; and (6) what is the relationship—if any—of climate change on type of bottom waters?

2. Case History

The pelagic sediments of five Tethyan localities (Figures 1 and 2) in the Umbria-Marche Basin (Central Apennines; Furlo, Contessa, Monte Petrano, and Le Brecce sections) and Belluno Basin (Southern Alps; Cismon section) in Italy were studied. During the late Albian–early Turonian time interval, both basins were located in the southern part of the Tethys Ocean, in the northern tropical climatic belt [*Dercourt et al.,* 2000; *Skelton et al.,* 2003]. High-resolution lithostratigraphy of these nicely exposed sections was described by *Gambacorta et al.* [2014], while integrated chemostratigraphy and biostratigraphy were documented by *Gambacorta et al.* [2015].

The Umbria-Marche Basin, located today in the central-eastern part of Italy, represents a unique place where an almost continuous Jurassic to Oligocene pelagic sequence is well preserved. The Umbria-Marche

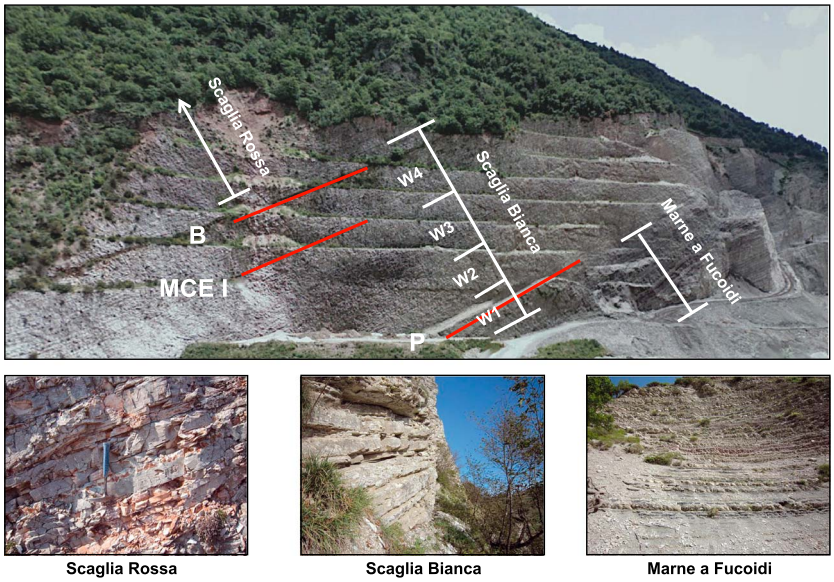

Figure 3. Scaglia Bianca subdivision in members as described by *Coccioni et al.* [1992] and *Coccioni and Galeotti* [2003]. (top) Taken from the Contessa Highway right in front of the Contessa outcrop (Vispi quarry), the transition to the (bottom left) Marne a Fucoidi Formation and the Scaglia Rossa Formation (Figure 3, top) is clearly visible. The three major events described in this paper are highlighted in red: P, Pialli or Breistoffer Event (OAE1 d); MCE I, Mid Cenomanian Event I; and B, Bonarelli (OAE 2). In the lower part, from left to right, the close-ups of the Scaglia Rossa (Monte Petrano), Scaglia Bianca (Monte Petrano) and Marne a Fucoidi (Le Brecce) are shown.

sequence was entirely deposited on the continental crust of the Adria microplate, in a "basins and swells" setting with a complex paleobathymetry [*Alvarez*, 1990]. The latest Albian–early Turonian time interval is represented by the Scaglia Bianca Formation, a mainly calcareous pelagic sequence resulting from lithification of nannofossil-planktonic foraminiferal oozes [*Arthur and Premoli Silva*, 1982] deposited at bathyal depths. The Scaglia Bianca lies above the Marne a Fucoidi Formation (lower Aptian–upper Albian) and is followed by the Scaglia Rossa Formation (lower Turonian–middle Eocene). The Scaglia Bianca Formation was informally subdivided into four members, as reported in Figure 3 [*Coccioni et al.,* 1992; *Coccioni and Galeotti*, 2003].

The Furlo section is located in the homonymous gorge, 25 km southeast of Urbino and is part of an abandoned quarry [*Beaudoin et al.,* 1996; *Turgeon and Brumsack*, 2006; *Mitchell et al.,* 2008; *Turgeon and Creaser,* 2008; *Lanci et al.,* 2010]. The upper Albian–lower Turonian measured sequence is 30 m thick (Figure 2). The Contessa outcrop is located about 2 km from Gubbio in the Vispi active quarry close to the homonymous highway that gives the informal name to the outcrop [*Monechi and Parisi*, 1989; *Coccioni and Galeotti*, 2003; *Tsikos et al.,* 2004]. The interval of interest is 29 m thick (Figure 2). As an additional data set, the Gubbio 2 Core collected from a borehole drilled right next to the Contessa outcrop during the C/T-Net research project [e.g., *Tsikos et al.,* 2004] has been redescribed, correlated to, and integrated with the outcrop data. The 20 m thick section at Le Brecce (Figure 2) is located inside a gorge, at 3 km west from the Piobbico village. The studied outcrop is at the km 34 of the state road 257-Apecchiese, close to the Piobbico drill site [*Tiraboschi et al.,* 2009]. The 90 m thick section at Monte Petrano (Figure 2) is about 2 km east of the Moria village [*Giorgioni et al.,* 2012].

The 60 m thick Cismon section (Figure 2) is located in the Venetian Southern Alps, northeastern Italy, along the SS50 (State Highway 50) not far from the village of Lamon and along the Cismon stream [*Channell et al.,* 1979b; *Bellanca et al.,* 1996]. During the Cenomanian the Cismon area was located close to the hinge between the Trento Plateau and the Belluno Basin [*Erba and Larson*, 1998]. The Cenomanian Scaglia Variegata Formation [*Channell et al.,* 1979a] was deposited in a "horst and graben" extensional setting [*Bernoulli and Jenkyns*, 1974; *Bosellini et al.,* 1978; *Winterer and Bosellini*, 1981] with the alternation of yellowish to grey limestones, chert bands and shales/black shales [*Channell et al.,* 1979b; *Claps et al.,* 1991; *Claps and Masetti*, 1994; *Bellanca et al.,* 1996].

Table 1. Facies Association of the Studied Successions (Modified After *Gambacorta et al.* [2014])

Facies Code	Facies Name	Major Characteristics	Interpretation
A0	Marl/Marlstones/ Mud/Mudstones	Homogeneous to composition-laminated marlstones, light brown, light grey up to purplish/green coloured. Rare clayey marlstone layers also occur. Both seams (less than 1 cm thick) and layers are present ranging from 1 cm to about 30 cm.	Mixing of biogenic, indigenous particles with allochtonous clays (eolian, fluvial, and volcanic ash) or from hydrothermal sources, settled under normal oxygenation conditions at the sea bottom.
A1	Homogeneous marly limestone	Light coloured marly calcilutites, with 60 up to 80% of micrite, forming millimeter- to centimeter-thick layers with gradual boundaries.	Settling under normal-oxygenated conditions. Clay percentage varies owing to changes in carbonate input.
A2	Homogeneous limestone	Structureless to pervasively mottled calcilutites (mudstones and wackestones), forming thin beds with flat to undulating boundaries, ranging from reddish, grey, to yellowish/grey in colour.	Settling to an oxygenated sea bottom and homogenized by pervasive mottling.
A3	Radiolarian layer	Siliceous structureless layers, millimeter to centimeter thick with gradual boundaries, mainly consisting of spumellarian specimens.	Radiolarian ooze settled under eutrophic conditions on an oxygenated sea bottom
A4	Alternating micritic and organic-rich laminasets	Alternation of wackestones and mudstones with abundant organic matter flakes or concentrations, forming plane-parallel laminated layers, up to 1 cm thick, underlaying the black shales and rarely also the black cherts.	Compositional lamination formed by settling at the onset of dysoxic/anoxic conditions.
A5	Black shale	Organic-rich shales, forming some millimeter up to about 5 cm thick layers. Carbonate content varies from 20% to 80%. Thin pervasive compositional lamination with large TOC and carbonate content variations.	Settling under dysoxic/anoxic/euxinic sea bottom conditions.
B2	Marly-limestone bed	Very thin to thin marly-limestone beds with sharp to erosional base and faint internal lamination, usually grey and always slightly darker in color than the embedding layers due to a slightly higher concentration of clay.	Settling plus mild current winnowing and redistribution during discrete episodes of weak traction by bottom currents under oxygenated sea bottom conditions.
B3	Laminated radiolarian beds	Very thin, partly silicified, faintly laminated beds with sharp boundaries. Radiolarian-rich and clay rich laminae alternate in these grey layers.	Traction by bottom currents and deposition in shear stress sheltered pools or during times of waning bottom currents. The B3 laminated radiolarian beds might be equivalent to the B2 facies in terms of shear stress.
C2	Limestone with pervasive plane-parallel lamination	Every lamina has a sharp contact both at the base and at the top. The thickness of the laminae varies between about 1 and 15 mm, and their separation varies between about 2 and 10 mm. The laminae are internally homogeneous and lack almost completely of larg	Erosion, reworking, and redistribution by bottom currents in an oxygenated depositional setting under increasing shear stress conditions compared to facies B2/B3.
D2	Limestone with oblique and wavy lamination	2–20 cm thick foraminiferal wackestone beds with wavy top and sharp erosional bottom. Curve and oblique lamination is accompanied by erosive contacts between the laminasets. Mud offshoots and clayy-rich laminae are common, and include silt- to sand-size	Small-scale, low-relief bed forms, migrating under variable shear stress conditions, higher than compared to facies C2.
E2	Foraminiferal-intraclastic lag	Concentrations and/or alignments of large foraminifera and/or, more rarely, intraclasts to form flat lenses or laminae of packstone/wackestone and float stones, frequently embedded with abrupt base within the C2/D2 facies.	Foraminiferal-intraclastic lags, generated by the removal by winnowing of the fine fraction under oxygenated conditions.

Table 1. (continued)

Facies Code	Facies Name	Major Characteristics	Interpretation
G1/G2/G3	Reddish/pink/grey chert band	Diagenetic facies characterized by the massive concentration of radiolarian tests. Normally vitreous and structureless, the thickness of the chert bands, with sharp boundaries, can vary from about 0.5 cm to about 20 cm.	Diagenetic analogue of the radiolarian layer (A3). The difference in color among G1, G2, and G3 (and G4) is interpreted as the result of different original content in organic matter and iron and redox conditions.
G4	Homogeneous black chert band	Black chert bands with the same features of G1, G2, G3 diagenetic facies.	G4 cherts represent deposition of siliceous remains under dysoxic/anoxic/euxinic sea bottom conditions.
G4a	Bedded black chert band	Thin alternation of silicified shaly organic-rich beds and radiolarian-rich horizons with an erosive base.	Compositional alternation of mainly settled organic-rich shales with winnowed radiolarian horizons under prevailing dysoxic/anoxic/euxinic sea bottom conditions.
R1/R2	Graded-laminated limestones	Graded to laminated calcarenite-calcislitite-calcilutite beds (R1) and calcisiltite-calcilutite beds (R2) with a flat, sharp base, from 0.1 cm to about 3 cm thick. R1 and R2 beds consist of graded foraminferal wackestones, with plane-parallel lamination	Fine-grained pelagic turbidites. According to the grain size a sand- to silt-sized pelagic turbiditic bed (R1) and silt- to mud-sized highly diluted pelagic turbiditic bed (R2) are distinguished.
Ha	Wavy-bedded and pseudo nodular limestones	Thin beds of pale grey mudstones/wackestones with nonparallel, undulating boundaries.	Diagenetically enhanced wavy bedding associated with extremely low sedimentation rates and or some sediment removal
Hb	Wavy and hummocky bedded limestones	Pale grey, alternating wackestones and mudstones, with hummocky boundaries and disturbed bedding	Soft sediment deformation under shear stress by sea bottom currents.

3. Methods

3.1. Data Collection

The five selected sections were logged at millimeter scale. Facies analysis is based on the description of texture, composition, sedimentary structure, shape, and features of the bounding surfaces of layers and beds (either depositional/erosional or diagenetic), complemented by microfacies analysis on thin sections and peels from selected facies. This full array of data could not be collected within the Bonarelli Level due to sample preparation difficulties that prevented full petrographic and microtextural analyses. Hence, the Bonarelli Level data set includes the field sedimentological description (bedding types, internal structures, and composition). Field and laboratory facies description led to the identification of a number of facies types interpreted in terms of depositional and lithogenetic processes (Table 1). This facies association was presented and thoroughly described in a previous paper [*Gambacorta et al.,* 2014], which highlighted the repetitive association of purely pelagic oozes with an array of facies derived from bottom current shear, traction, redistribution, and winnowing of the seafloor sediments (from B2 to E2, G4a, and H in Table 1). In synthesis, the facies scheme of Table 1 shows the sedimentary products of the major controls on the pelagic environment that could be identified in this setting, acting both on the water column and at the sea bottom: nutrients, oxygenation, fine-grained input, and current activity (see Table 1 for a summary of facies descriptions and the relative interpretations).

3.2. Data Analysis

In the scheme of Figure 4 the facies responding to sea bottom oxygenation conditions, bottom currents strength, and nutrients availability were plotted according to these parameters (on the left hand of the central bar the facies related to oxygen depletion, i.e., black shale and black chert layers, Table 1, on the right side all the facies related to "normal" oxygenation conditions). Moreover, specific care has been devoted to distinguish the sedimentary facies derived from pure settling processes, controlled by the oceanographic factors (primary productivity, oxygen deficiency, and bottom water ventilation) and external inputs (either aeolian or volcaniclastic and/or turbiditic; Table 1) from the deposits affected by current redistribution (Figure 4).

Carbon and oxygen isotopic data, integrated with nannofossil biostratigraphy, allowed precise dating and correlation of the selected sections [*Gambacorta et al.,* 2015]. The distinctive positive excursions of

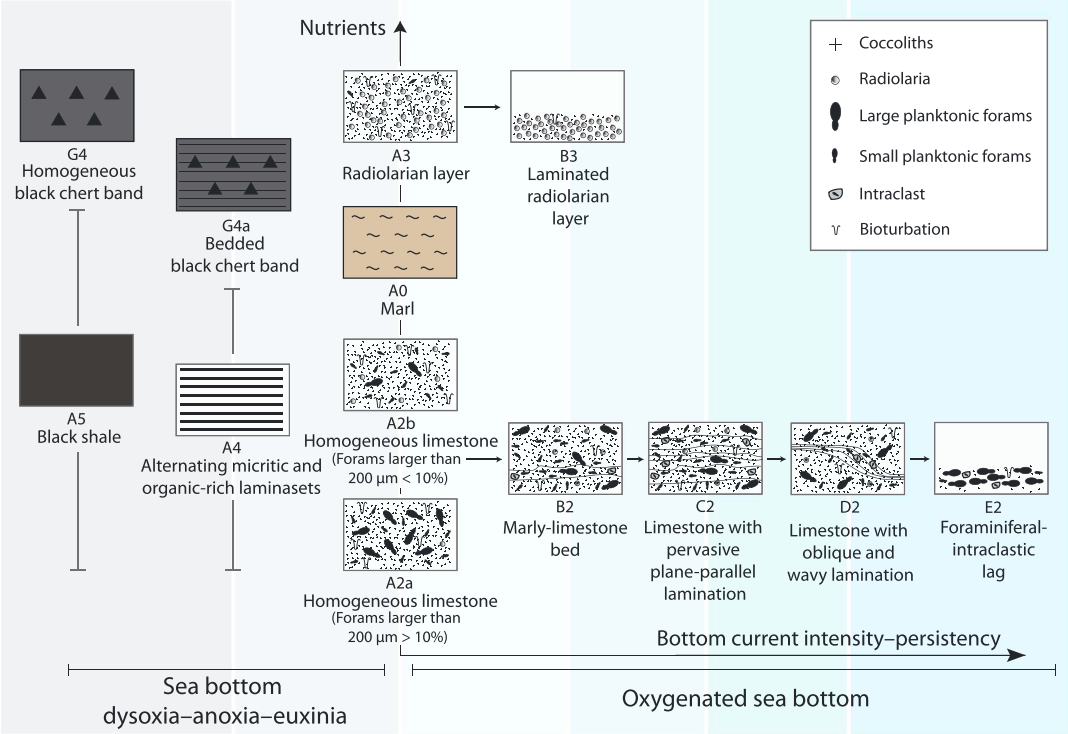

Figure 4. Facies scheme representing the ideal transition from (left) anoxic to (right) oxygenated facies. Two transitional facies alternating micritic and organic-rich laminasets and bedded black chert bands, as described in *Gambacorta et al.* [2014] are distinguished. From left to right all the facies are organized with increasing intensity of the sea bottom currents shear stress. See legend for symbols explanation.

OAE 1d (latest Albian), the MCE I (middle Cenomanian), and OAE 2 (latest Cenomanian) were unambiguously identified. Comparison with the stratotype section at Pueblo (Colorado) and other classical litho-chemo-biostratigraphic records allowed the identification of hiatuses in the studied sections [*Gambacorta et al.*, 2015]. In particular, detailed $\delta^{13}C$ profiles through the Bonarelli Level detected 160–510 kyr long hiatuses eliding the middle to upper part of the characteristic carbon isotope excursion and part of the following interval.

We apply the stacking pattern concept to the studied sediments considering that the superposition of specific bed types, belonging to the categorized facies, responds to the controlling factors on sedimentation in the pelagic domain, hence permitting the recognition of environmental changes through time at any fixed point. The repetition of four basic types of stacking patterns identifies the lithogenetic processes that cooperate under the oceanographic controls in the pelagic environment.

For every studied section a composite log was realized (Figure 5 as an example—all the detailed composite logs of the studied sections are reported in supporting information S1). In the case of the Bonarelli Level only the lithofacies log (Figure 6) was derived from detailed field lithotextural and sedimentological information. In these figures, the left panel is the comprehensive schematic log with the vertical lithologic variations, distinguishing whitish or reddish limestones from black shales and reporting the differently colored continuous chert bands. The right panel reports all the additional features in the form of a range chart, where the presence and persistence of a specific feature is indicated by a black bar. The following features are reported, from left to right: Position of redeposited layers (facies R as defined in Table 1), hardgrounds, chert nodules, cherty intervals, radiolarian layers, marl beds thicker than 0.5 cm, intervals with discrete bioturbation, pyrite nodules, and sparse lined forams. Concerning bioturbation, we have chosen to split it into two qualitative different classes: A moderate "discrete" bioturbation class for the cases where the traces are rare to common within the described interval and an intense discrete bioturbation class when the abundant traces dominate a vast area of the investigated interval. The latter is represented in the panel with a black bar larger than the one used for the less intensely bioturbated intervals.

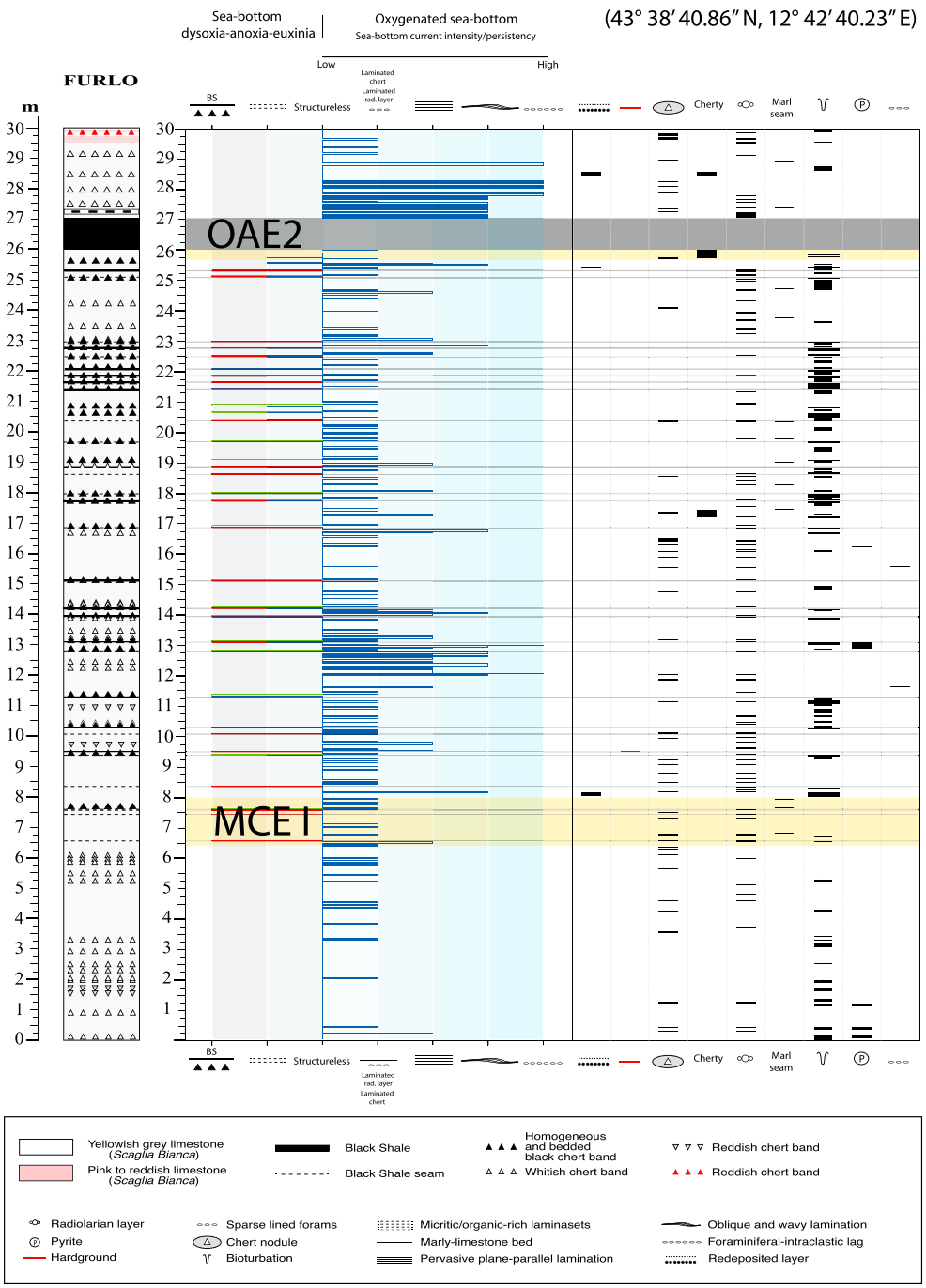

Figure 5. Furlo composite section, see text for explanation. The position of the Bonarelli Level is indicated by a grey band while the OAE 2 and MCE I interval by a yellow band. The composite logs of all the other studied sections are reported in Supporting Information S1.

The central panel is the facies log where the facies stacking patterns are plotted on the vertical axis, according to the classification of Table 1, as a function of bottom current activity/intensity and sea bottom oxygenation, (*x* axis), following the scheme of Figure 4. The main aim of the central panel log in the section composite logs is to show synthetically the facies variations through time, as a function of the shear stress eventually exerted by bottom currents with respect to the bottom water oxygenation (as described in Table 1). We consider this plot as a proxy of the variability of bottom current intensity/persistency (see also *Gambacorta et al.* [2014] for the sedimentological details). The logs

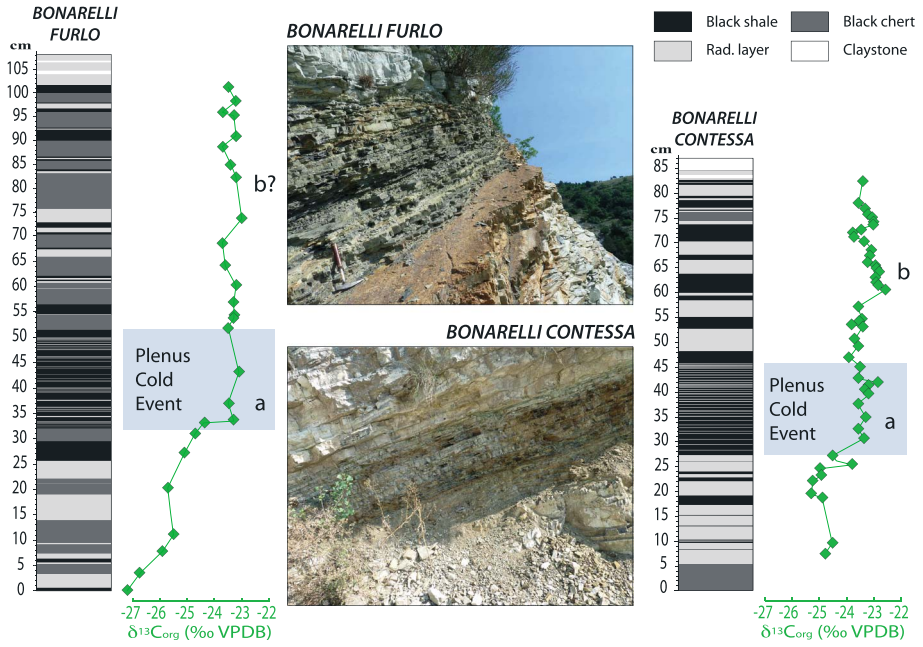

Figure 6. Field sedimentological log of the Bonarelli Level at Furlo and Contessa outcrops. Organic carbon isotopes for Furlo [*Gambacorta et al.,* 2015] and Contessa (Gubbio 2 Core) [*Tsikos et al.,* 2004] are reported next to lithological logs. The approximate position of the Plenus Cold Event [*Jarvis et al.,* 2011] is highlighted by a blue pattern. See text for explanation.

reported in supporting information S1 represent a summary of the data set that permitted to recognize the SP types and their recurrence through the stratigraphic columns.

4. Results

Based on facies association summarized in Table 1 and Figure 4, we differentiate the "settled" facies (background sedimentation) from the "current-related" facies, the latter represented by current-reworked and/or redeposited beds ("pelagic contourites") [*Gambacorta et al.*, 2014] that are plotted to the left of the central column in Figure 4. In the same plot of Figure 4, based on increasing nutrients and fine-grained siliciclastic (and/or volcanic input), the settled limestone facies grade to settled marlstone-shale facies and to siliceous (radiolaria-dominated) facies (moving upward along the *y* axis in Figure 4). Considering the oxygenation conditions of the sea bottom, the facies indicative of normal oxygenation (to the right in the plot of Figure 4) grade to oxygen deficiency-related facies, i.e., black shales and black cherts, at the left side of the same plot. Between them, two transitional facies of alternating micritic and organic-rich laminasets and bedded black chert bands (Figure 4, Facies A4 and G4a, respectively; Table 1) are reported. The diagram permits to read the facies transitions as a consequence of the changing controls. As it will be described later on (section 4.1), the facies stacking patterns will permit to link these transitions to time, revealing the depositional themes. On increasing traction intensity and normal oxygenation, the facies shift from homogeneous limestone (A2a) to single marly-limestone beds (B2), limestones with pervasive plane-parallel lamination (C2), limestones with oblique and wavy lamination (D2), and then to foraminiferal-intraclastic lags (E2) (Table 1 and Figure 4). Within this array of tractive facies we include also the micrites with few sparse foraminifera lined by feeble bottom currents (belonging to B2 facies in Table 1), the laminated radiolarian layers (B3), and the laminated chert bands (G4a), indicating the effect of very weak traction intensity.

We underline that the 50 cm thick interval immediately above the Bonarelli Level is characterized by high silica content, hampering the analyses of thin sections and peels. Pervasive parallel laminations were observed in this interval at the field observation scale, but, due to the above mentioned technical limits, limited microfacies observation was done in order to safely exclude a mere compositional origin of the laminae. In the composite logs (Figure 5 and supporting information S1) this cherty interval has been interpreted as a tractive, pervasive parallel laminated interval (facies C2 as defined in Table 1).

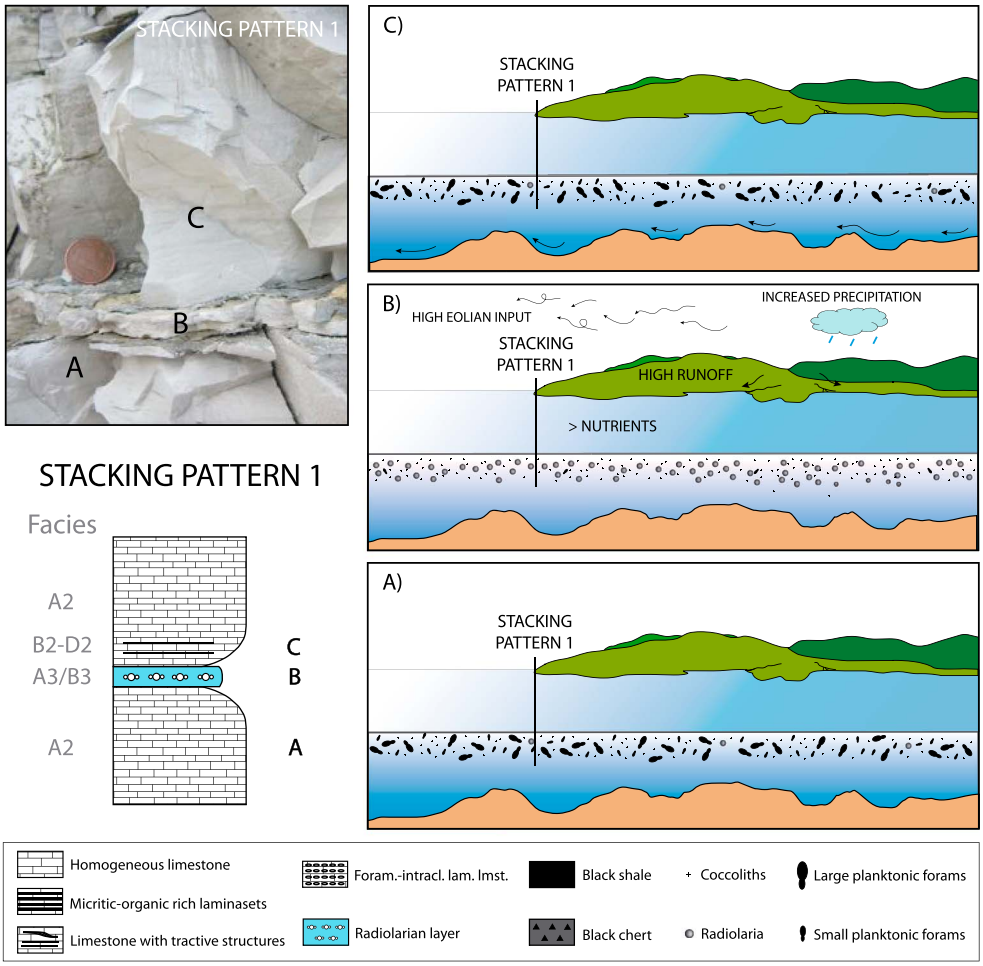

Figure 7a. Limestone-radiolaria-limestone sequence (Stacking Pattern 1). (right) Depositional model for Stacking Pattern 1. Facies labels as described in Table 1. In some cases the marlstone layers of the A0 facies can replace the radiolarian layers (facies A3). See text for a detailed explanation.

4.1. Stacking Patterns

In the studied successions, four SP types were identified, thus suggesting repetitive processes at their origin. These are graphically presented in Figures 7a–7d.

SP1 (Figure 7a): In the studied sections the most common SP consists of repetitive cycles of homogeneous calcilutite layers (facies A2), recurrently coupled with marlstone layers (facies A0), followed by radiolarian layers (facies A3/B3), limestone beds with traction structures (facies B2–D2) and a new homogeneous calcilutite layer (facies A2). In some cases the marlstone layers of the A0 facies occupy the same position of the radiolarian layers (facies A3).

We interpret this pattern as due to cycles of fertilization under oxic conditions at the seafloor. During times of normal oligotrophic conditions the main producers are coccolithophorids and foraminifera forming a carbonate ooze (facies A2; Figure 7a). During times of increased nutrient availability, eventually due to enhanced riverine input or alternatively related to upwelling loops or to intensified surface water mixing, the productivity is dominated by siliceous organisms with the deposition of a radiolarian layer (facies A3/B3; Figure 7a) in an environment reasonably characterized by feeble bottom currents. The traction structures in the limestone above the radiolarian layer (facies B2–D2; Figure 7a) suggest that efficient circulation is progressively reactivated. When also oligotrophic conditions were established, deposition of the settled calcareous ooze (A2 at the top of the facies stack; Figure 7a) replaced the bottom current-related facies.

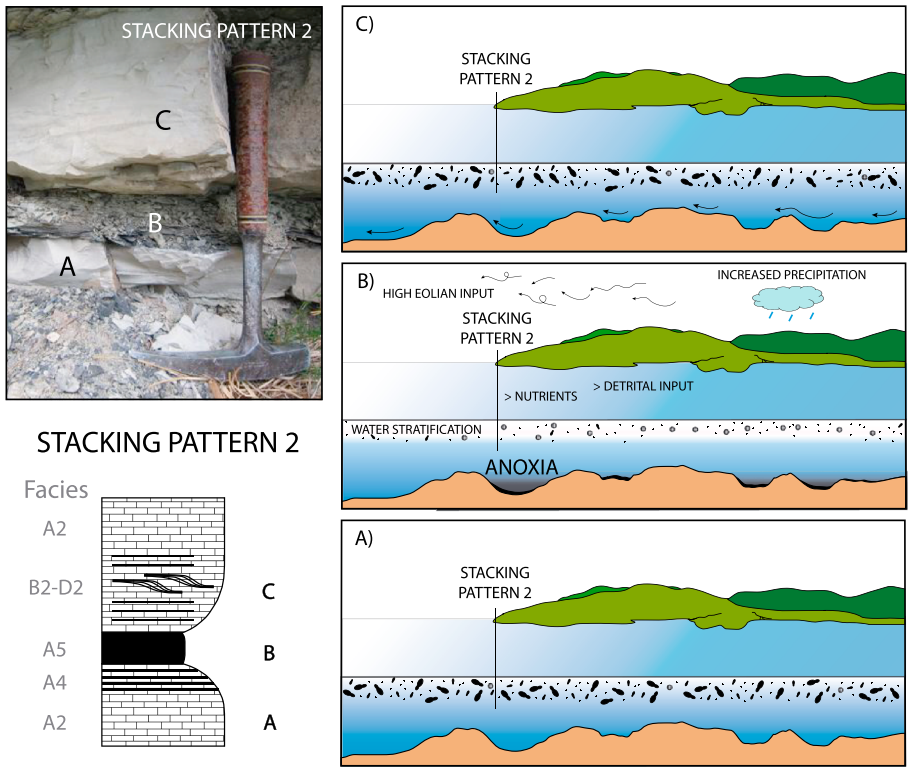

Figure 7b. Limestone-black shale-limestone sequence (Stacking Pattern 2). (right) Depositional model for Stacking Pattern 2. Facies labels as described in Table 1. See text for a detailed explanation.

This kind of stacking pattern, representing oxygenated bottom waters with prevalent settling ("background sedimentation"), is the most diffuse and typical of both the Umbria-Marche Basin and the Belluno Basin throughout the whole stratigraphic sequence. The occurrence of the A0 facies in SP1, below the siliceous layers or "replacing" them, implies a lowering of the compositional micrite/clay ratio of the layers along the stacking pattern, from the facies A2 calcilutites to the A0 marlstones. This micrite decreasing trend can culminate into a siliceous layer (facies A3) when the carbonate content is at its minimum and the clay content is diluted by the preponderant silica. The significance of this interpretation in the frame of the environmental changes will be discussed later on (section 5.1).

SP2 (Figure 7b): This SP is recurrent in the intervals characterized by the presence of a black shale and absence of black cherts. The most general expression of SP2 is characterized by a settled calcilutite at the base (facies A2) that grades first to micritic intervals alternatively rich and poor of organic matter (facies A4) and then to a black shale (facies A5). Tractive beds of whitish limestone (facies B2–D2) follow upsection and are capped by a settled calcilutite (facies A2) at the top of the SP.

The SP2 indicates that starting from oxygenated conditions (A in Figure 7b) the onset of dysoxia-anoxia (B in Figure 7b) occurs gradually. The re-establishment of oxic conditions is accompanied by a phase of enhanced bottom water circulation (C in Figure 7b). SP2 is characteristic of the Pialli Level of the Umbria-Marche Basin (Le Brecce and Monte Petrano sections; Figure 1; see supporting information S1).

SP3 (Figure 7c): This SP forms two slightly different sequences, namely, SP3a and SP3b, that share the presence of a black chert band in their core. From bottom to top SP3a (Figure 7c) is characterized by: Settled whitish calcilutite (facies A2), black chert band (facies G4 or G4a), laminated limestone (facies B2–D2) and then back again to a light colored, settled calcilutite (facies A2). The sequence of SP3b (Figure 7c) is quite similar, being characterized from bottom to top by Settled homogeneous calcilutite (facies A2), alternated micritic and organic-rich laminasets (facies A4), a black shale (facies A5), a homogeneous or bedded black chert band (facies G4 and/or G4a), laminated limestone beds (facies B2–D2) before getting

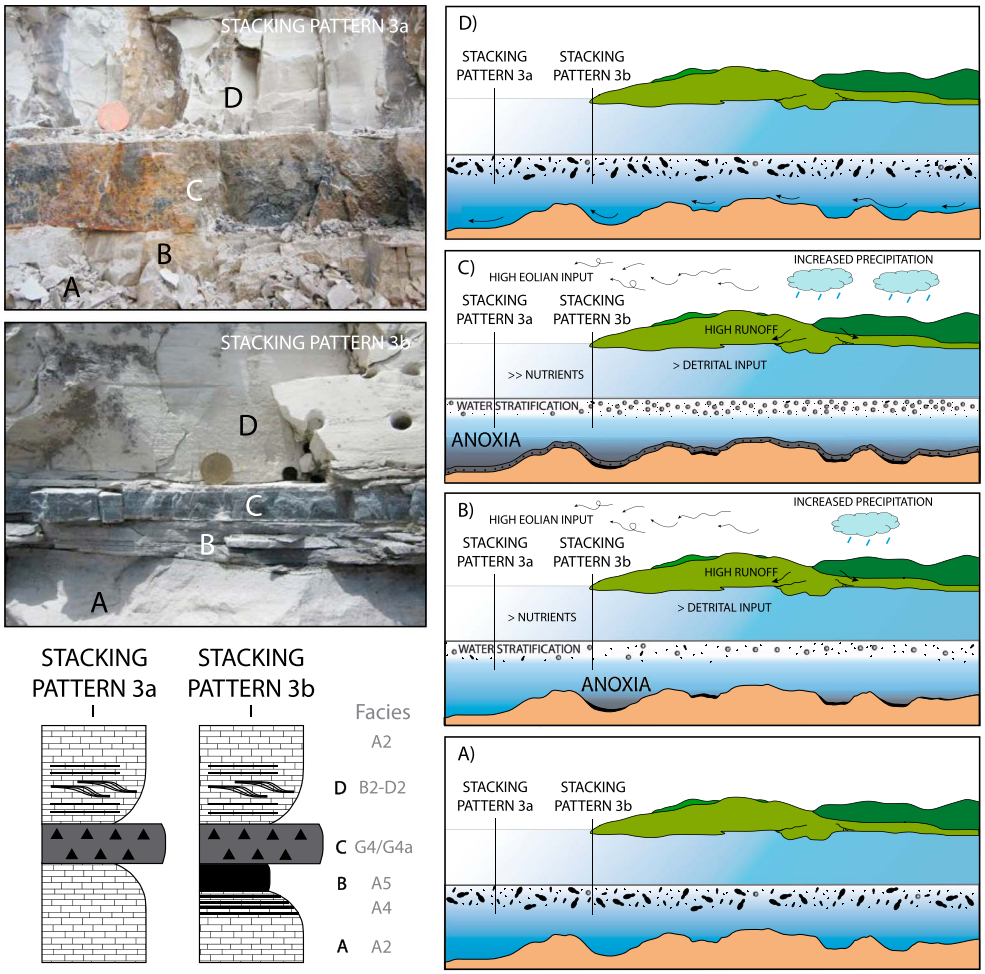

Figure 7c. Limestone-black shale-black chert-limestone sequence (Stacking Pattern 3a and 3b). (right) Depositional model for Stacking Pattern 3a and 3b. Facies labels as described in Table 1. See text for a detailed explanation.

back again to a homogeneous limestone (facies A2). The black shale can be represented either by a centimeter-thick layer or just by a black shale seam only a few millimeters thick.

SP3 occurs in the upper part of the studied successions above the mid-Cenomanian event I up to the Bonarelli Level (Figure 2). In particular, this stratigraphic time interval at Furlo and Monte Petrano (see supporting information S1) is almost completely characterized by SP3b while at Contessa and Cismon (see supporting information S1) by exclusively SP3a.

The superposition of black shales and black chert bands was already described by *Beaudoin et al.* [1996] and *Salmon et al.* [1998]. In the studied outcrops, black chert bands were distinguished in two main facies: When vitreous with no evident structures, they were defined as "homogeneous" (facies G4), while when characterized by a millimeter-scale alternation of silicified shaly organic-rich beds and radiolarian-rich horizons, they were described as "bedded" (facies G4a). Bedded black chert bands are common in Umbria-Marche Basin, while they are absent at Cismon.

We interpret SP3a and SP3b as the sedimentary expression of the same depositional processes at different basin locations during the shifts from oligotrophic to mesoeutrophic and anoxic conditions. The black chert core of both SP3a and SP3b relates to concurrent anoxia and high silica productivity (relevant availability of nutrients, owing to either enhanced riverine/aeolian input, similarly to Albian rhythmic black shales as suggested by *Tiraboschi et al.* [2009], or to upwelling conditions). The black shale that predates this interval in SP3b can be found only at some specific sites (Furlo and Monte Petrano; see supporting information S1), suggesting a local physiographic control. There is no enough circumstantial evidence of deposition into a

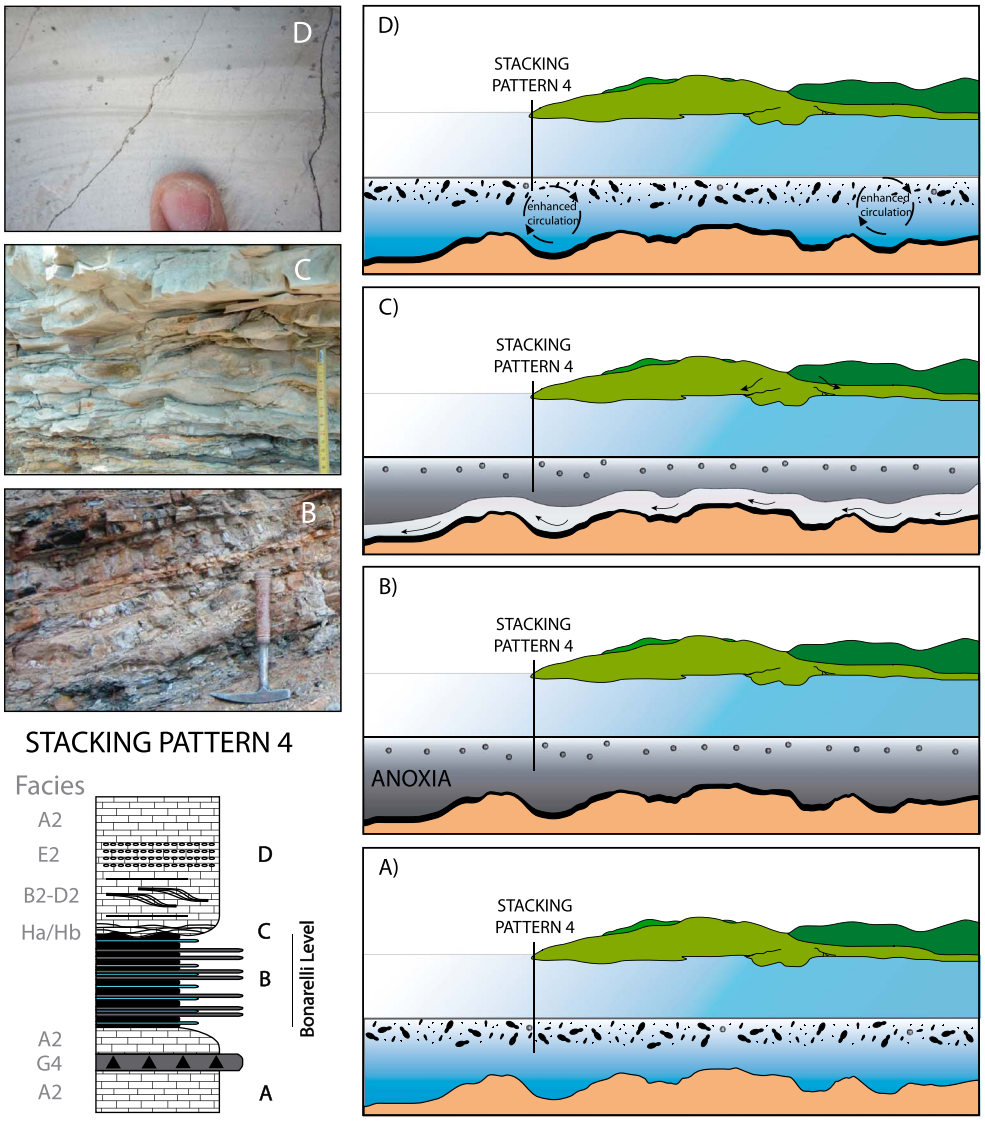

Figure 7d. Stacking pattern characterizing the interval right below and above the Bonarelli Level in the Umbra–Marche Basin (Stacking Pattern 4). Pictures C show the wavy and hummocky-bedded limestone facies (Hb in Table 1) at Furlo. (right) Depositional model for Stacking Pattern 4. Facies labels as described in Table 1. See text for a detailed explanation.

normal-faulted basin trough at these sites [*Alvarez*, 1990], so we can only presume that clay could have been trapped preferentially at these locations with a ponding effect in such a setting. Differently, in a more open and elevate setting (like a swell or a marginal ramp), clay could not be trapped, giving origin to SP3a (Contessa and Cismon settings; see supporting information S1). It should be also observed that SP3b is quite similar to SP2, with the addition of the black chert band. This could suggest that SP3b represents a transition from SP2 and SP3a, as a consequence of a shift from higher input of nutrients, during enhanced riverine input from land or toward upwelling-dominated conditions. This latter explanation cannot be excluded but does not justify the difference between the SP3a- and the SP3b-dominated settings. In order to explain all the observed features, it looks reasonable to consider the local basin physiography, too. Whether the combination of these two interpretations might lead to recognize a gradient of detrital input versus nutrients [*Lalli and Parsons*, 1997] moving from the SP3b-dominated settings to the SP3a-dominated environments and whether it represents a proxy of a proximal-distal gradient with respect to land and to the maximum expansion of the floating freshwater deltaic plumes entering the basin are impossible to ascertain, because of the poor knowledge about the paleophysiography of the basins. In any case SP3 (a and b) documents the shift from oxic and oligotrophic

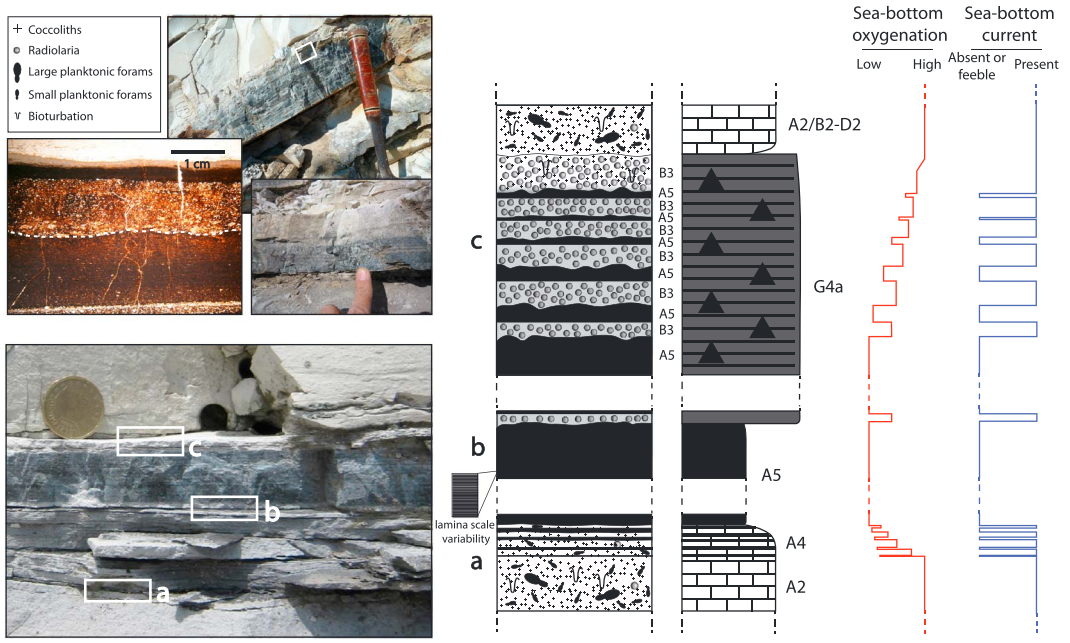

Figure 8. Lamina-thin bed-scale variation within Stacking Pattern 3b. (bottom left) Picture of a stacking pattern b on outcrop. (top left) Picture of a bedded black chert band and thin section of the interval surrounded by the white frame. (right) Sea bottom oxygenation conditions and presence of bottom-currents are ideally sketched on the right. Letters from a to "c" refer to the intervals highlighted in the picture in the lower left part of the figure.

conditions to anoxic and eutrophic conditions followed by the environmental resilience driven by a perturbation of the current circulation patterns.

Within SP3, the significance of black cherts, both homogeneous and bedded, deserves some additional remarks (Figure 8). Homogeneous black chert (facies G4, see Table 1) is the result of the deposition and preservation of organic matter during times dominated by biogenic silica production and minor terrigenous input. The resulting lithology is thus the siliceous analogue of a black shale. Bedded black chert bands (facies G4a, Table 1) are, instead, compositional alternations of radiolarian laminae, winnowed under the action of weak bottom currents and settled organic-rich shales. This facies G4a represents the condensed equivalent of a silicified alternation of black shale and radiolarian layers (facies A5 and B3 as defined in Table 1). It forms during prevailing anoxic bottom waters punctuated by traction/winnowing events, with a progressive shift from anoxic to dysoxic and finally oxic conditions. Probably, this facies is the small-scale expression of the large-scale alternation of chert beds and shale intervals described by *Hori et al.* [1993] resulting from cyclic rapid accumulation of biogenic SiO_2 under extremely slow accumulative environments of shale. The intriguing millimeter-scale variability within the sequence suggests that the onset, transition, and recovery from anoxia does not occur at once but is a continuous subtle variation of mutually linked processes (Figure 8).

SP4 (Figure 7d): Through all the Umbria-Marche sections, wavy bedded and pseudo nodular light grey limestones (Facies Ha in Table 1) occur just above the Bonarelli. Only at Furlo, the wavy and hummocky-bedded limestone facies (Hb in Table 1) form an interval about 15 cm thick above the Bonarelli top. The pseudonodularity of these Ha and Hb facies beds testifies the strong diagenetic modification of these limestones that however preserve some evidence of very low sedimentation rate and some sediment removal (Facies Ha) and local soft-sediment deformation (Hb), plausibly owing to shear stress by bottom currents. In all the Umbria—Marche sections, the wavy and pseudo nodular interval is followed by a some decimeter-thick intervals of plane-parallel and wavy-laminated siliceous beds, presumably representing strongly silicified laminated limestones, whose enigmatic microfacies does not preserve any prediagenetic feature. In all the sections but the Cismon (see supporting information S1), a thick interval of foraminiferal-intraclastic laminated limestones, resulting from the concentration and alignment of large planktonic foraminifera and some intraclasts to form flat lenses or laminae of packstone/wackestone and float stones (Facies E2, Table 1), occurs above the silicified layers. These beds, frequently embedded within the pervasive laminated and wavy facies

(C2 and D2, Table 1) with sharp contacts, represent residual lags produced by winnowing of the fine fraction in well mixed—well-oxygenated bottom waters. Moreover, in particular at the Furlo and Contessa sections, some feeble to pervasive laminae were observed in the cherty layers between the Black Marker and the base of the Bonarelli Level, thus suggesting the presence of at least weak bottom currents during the deposition of this interval.

Figures 7d and 6 show also the peculiar facies association of the Bonarelli Level. Due to difficulties with samples treatment a thorough definition of the stacking pattern internal to the Bonarelli Level could not be obtained. However, based on field observation, the tight association of repetitive black chert facies (G4 and eventually G4a in Table 1), radiolarian layers (A3 and B3 in Table 1), and black shales (A5 in Table 1) suggests that during the long-lasting anoxic conditions that accompanied the deposition of the Bonarelli Level variable trophic conditions occurred with tractive events punctuating the entire time span covered by the Bonarelli Level (Figure 6).

5. Discussion

5.1. Interplay of Surface and Bottom Water Masses

In the studied settled lithified oozes (facies A1, A2, and A3), the common components of all the identified SPs consist of nannofossils, calcite microparticles, planktonic foraminifera, rare benthic foraminifera, and radiolaria with some mudstone intraclasts and variable amounts of fine-grained siliciclastics (silt and clay) as minor components. The biogenic particles contribute to most of the bulk sediment composition, while clay represents a limited amount of particulate in the water column. Under mesotrophic to eutrophic conditions, K-strategist-dominated calcareous plankton is overwhelmed by r-opportunist diatoms and radiolarians [*Margalef*, 1978].

Among surface water parameters, nutrient availability determined the observed biogenic association as documented in previous studies of Mid-Cretaceous calcareous plankton [*Premoli Silva et al.,* 1999; *Leckie et al.,* 2002; *Erba*, 2004; *Mutterlose et al.,* 2005]. When trophic levels increased, nannoplankton assemblages became enriched in fertility-related species, typically producing small coccoliths and, therefore, inducing decreased biogenic calcite fluxes to the seafloor [e.g., *Erba and Tremolada*, 2004; *Erba*, 2006]. Planktonic foraminifera, with larger and more ornamented tests, proliferated under stable conditions, while small and thin planktonic foraminifera characterized times of unstable and mesotrophic conditions [*Premoli Silva et al.,* 1999]. As in modern oceans, siliceous plankton was the r-opportunist group during the Cretaceous [*Premoli Silva et al.,* 1999; *Leckie et al.,* 2002; *Erba*, 2004]. Thus, we can identify two antagonist biogenic factories that lead to different sediments: A "carbonate realm" and a "siliceous realm," as schematically represented in the "lithogenetic" scheme of Figure 9. The third component of the ternary compositional system is clay, controlled by changes in fine-grained input and/or change in carbonate accumulation controlled by the depth of the lysocline and the calcite compensation depth (CCD). Locking the clay input as a constant, how does the transition from the carbonate to the siliceous realms develop? As a matter of fact, in the analyzed successions, "layering" is mostly a diagenetic feature, due to both enhancing of compositional/textural changes and to segregation of clay, carbonate, and silica minerals along newly formed interfaces [see *Gambacorta et al.,* 2014]. On the contrary, it cannot be denied that even considering a diagenetic overprint, lithotype boundaries have to be related to primary depositional factors. The sharp changes from carbonate to siliceous sediments observed at the facies scale are plausibly related to changes in the trophic level with consequent changes in the dominant planktonic group. In this perspective, changes in surface water were coupled with changes in deep water conditions, eventually promoting also the regional shallowing of the CCD.

In the studied sections (see supporting information S1) the transition from a calcareous layer (facies A2) to a radiolarian layer (facies A3) is very frequent, as is documented by SP1 and SP3a. In many cases we observed a marlstone layer in between (facies A0), sometimes thicker than 1 cm, that is a thickness sufficient to exclude a diagenetic segregation origin. Seawater is above a critical undersaturation level in calcite above the CCD, while it is largely undersaturated in silica along the water column below some 500–1000 m. A high level of siliceous productivity is needed in order to allow the preservation from dissolution of siliceous tests during their settling through the water column and their deposition at the seafloor. Based on these facts, we

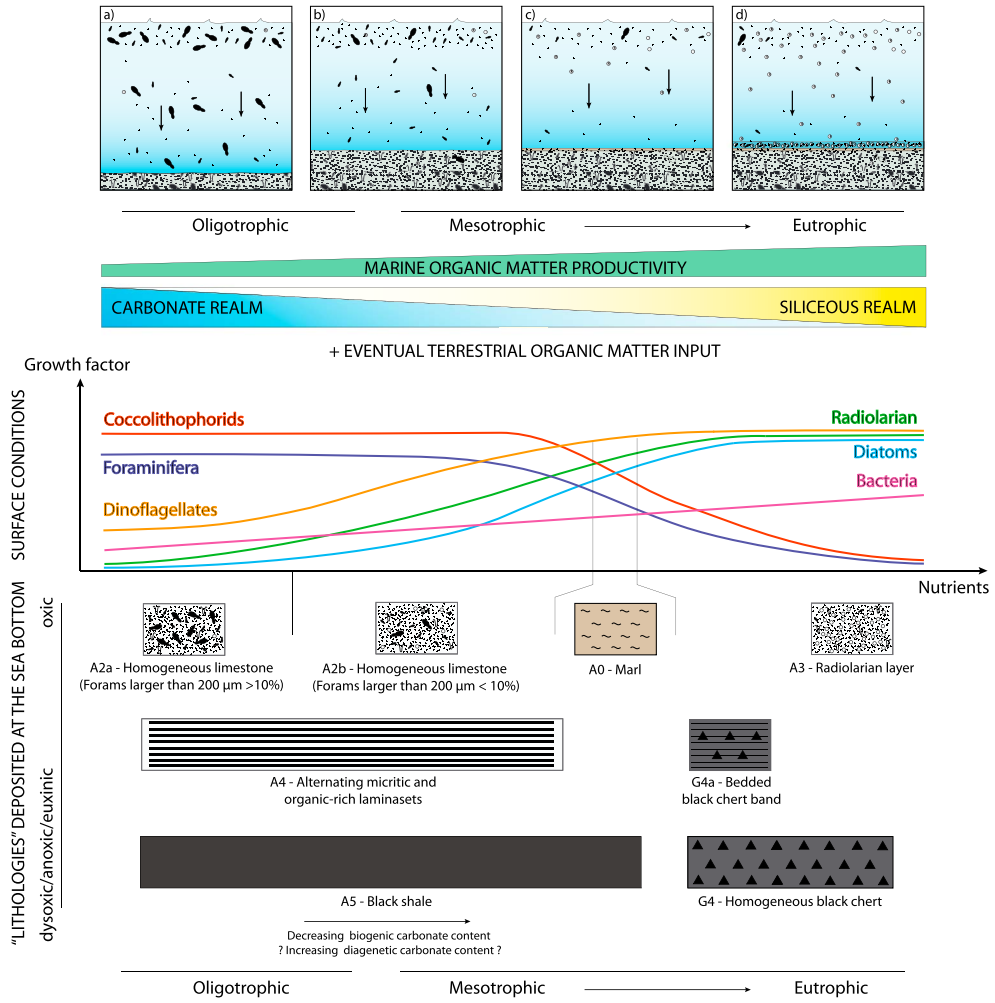

Figure 9. Conceptual scheme illustrating the relationship between the observed facies and the general paleoceanographic parameters of the pelagic environment during the shift from a carbonate- to a siliceous-dominated deposition (see text for a detailed explanation). Dinoflagellates, diatoms, and bacteria curves were sketched following, respectively, *Young* [1994] and *Horner-Devine et al.* [2003].

speculate that in a pelagic environment at least part of the observed marlstone layers (facies A0) are explainable as the result of different saturation states of calcite and silica along the water column, resulting in variable dissolution/preservation of carbonate versus siliceous particles.

With the exclusion of exceptional times of higher clay input due to increased riverine supply, and/or large amounts of aeolian dust or volcanic ashes, we can assume a continuous input of very fine grained terrigenous material (clay), diluted by the huge amount of biogenic carbonate (that means we "lock" the clay input, at this first interpretative model stage, as it was previously discussed). During times of gradual shift to mesotrophic/eutrophic conditions the carbonate producers decrease, while the increase of the silica producers is still insufficient to warrant their accumulation and preservation (Figure 9). The resulting lithology would be a marlstone/claystone facies that is the expression of a lower calcite sedimentation rate coupled with silica dissolution, thus mimicking condensation. In some cases, the marlstone layers could be the expression of a lower biogenic sedimentation rate, because of reduced rate of carbonate and silica production and higher rate of silica dissolution through the water column. Only when the increase in siliceous plankton is sufficient to prevail on silica dissolution the transition a siliceous-rich layer replacing the marlstone is indicated (Figure 9). If this does not occur, the stacking pattern contains a marlstone/claystone layer in its core. The corresponding perturbation implies a lowering of sedimentation rate during a more or less severe shift toward mesotrophic-eutrophic conditions in surface waters.

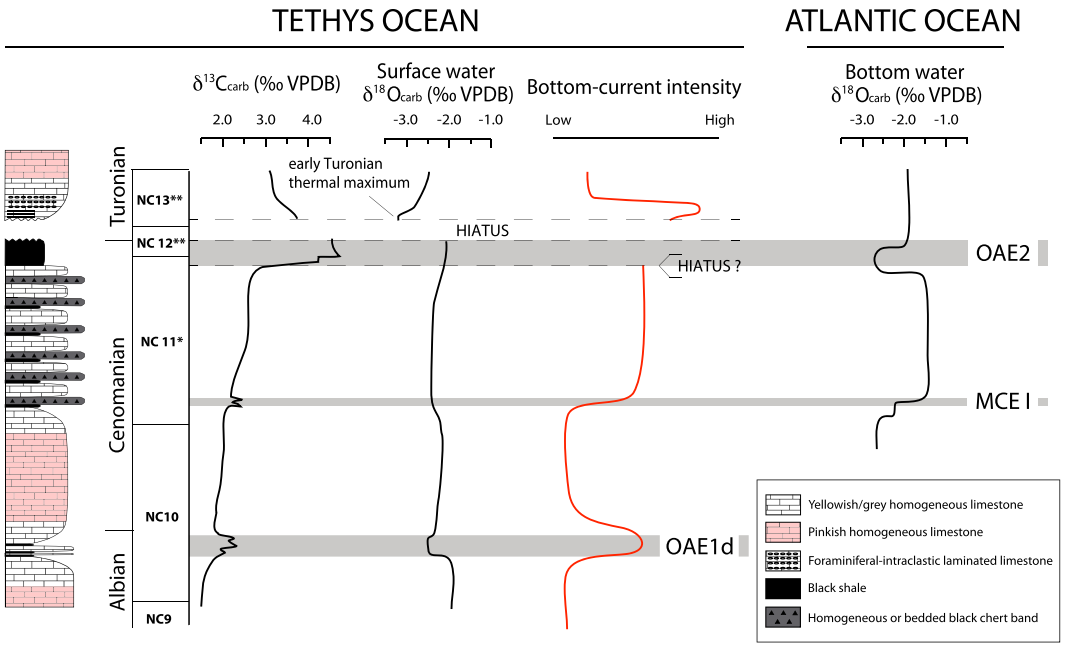

Figure 10. Schematic lithological profile, $\delta^{13}C_{carb}$, and $\delta^{18}O_{carb}$ profiles of the late Albian–lower Turonian sequence in the Umbria-Marche Basin. The reconstructed relative bottom current intensity based on facies vertical distribution is reported. On the right the $\delta^{18}O_{carb}$ record at Demerara Rise based on benthic forams [*Friedrich et al.,* 2008] is reported. The position of the Pialli or Breistoffer Event (OAE 1d), Mid-Cenomanian Event I (MCE I), and oceanic anoxic event 2 (OAE 2) is marked by a grey band. See text for a detailed explanation.

The above described processes are generally associated with well-oxygenated bottom water conditions (Stacking Pattern 1, Figure 7a). However, a comparable stacking pattern is observed for anoxic intervals, with the addition of preserved organic matter diluted within the hosting sediments (SP2 and SP3b, Figures 7b and 7c). We suppose a change from black shale (organic matter mixed with clay) corresponding to oligotrophic-mesotrophic and even to eutrophic conditions to a black chert (organic matter mixed with biogenic silica) corresponding to purely eutrophic conditions. Following this interpretation, black shales deposited under mesotrophic conditions can be considered as the equivalent of a relative condensed interval (during low mud input), due to both silica undersaturated waters and reduced carbonate accumulation/productivity, perhaps coupled with transient dissolution of the calcite fraction due to a shallowing of the lysocline.

According to the above described processes, variations in surface water trophic conditions would result in primary changes in facies and their stacking patterns at the seafloor, where the oxygen contents determined oxic to anoxic sedimentation. Such repetitive changes are then enhanced by the diagenetic overprint leading to thin, regular, and monotonous layering of pelagic successions.

5.2. Environmental Resilience and Sea Bottom Current Dynamics

The four observed SP types (Figures 7a–7d) are here interpreted as resulting from repetitive fluctuations from oligotrophic to eutrophic conditions and vice versa in surface waters. Such changes controlled the recurring variations from calcareous to siliceous-dominated biogenic sedimentation while the formation, flow, and intensity of bottom waters are a major contributing factor in determining oxic versus anoxic conditions at the seafloor. The observed SPs show that the recovery from black shales to oligotrophic and oxic conditions with deposition of a white calcareous ooze is normally associated to bottom currents, resulting in laminated and/or winnowed facies. The bottom current dynamics could either derive from basin-restricted processes or be driven by the global paleoceanographic evolution.

For the Furlo site, *Turgeon and Brumsack* [2006] proposed a partially silled physiography that could have enhanced the effect of water stratification. If so, we might assume that paleobathymetry and/or distance from the shore might have played a role in the distribution of the sediments corresponding to SP3b versus SP3a (see the corresponding discussion in section 4.1). In this perspective also the SPs at Monte Petrano,

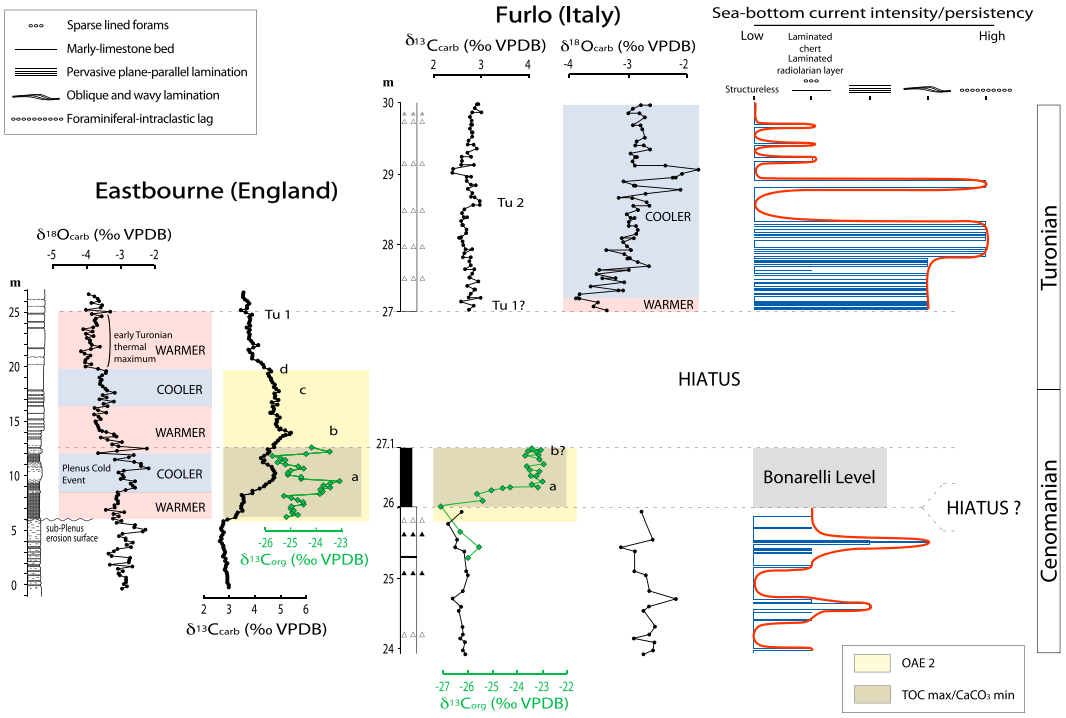

Figure 11. Comparison of the carbon ($\delta^{13}C_{carb}$ in black and $\delta^{13}C_{org}$ in green) and oxygen isotope profile for the OAE 2 interval at Eastbourne (England) [*Tsikos et al.,* 2004] and at Furlo [*Gambacorta et al.,* 2015]. The position of the Bonarelli Level is indicated by a grey band and the OAE 2 anomaly by a yellow band. Identification of $\delta^{13}C$ peaks for OAE 2, Tu 1 (Holywell Event), and Tu 2 follows *Voigt et al.* [2007]. On the oxygen isotope curves the warmer and cooler phases are highlighted with a pink and light blue pattern, respectively. The position of the so-called Plenus Cold Event and early Turonian thermal maximum is also indicated [*Jarvis et al.,* 2011]. On the right the reconstructed relative bottom current intensity (red line) based on facies vertical distribution (blue bars) is reported.

similarly to Furlo, although with thinner black shales, could suggest deposition in a restricted and/or proximal part of the Umbria-Marche Basin. The Contessa site, on the contrary, with its SP3a-dominated succession, was probably in a less confined or shallower setting.

Although, on one hand, the facies association and the SPs of the Scaglia Bianca document the activity of bottom currents and their role in the cyclicity of the depositional environment, on the other hand, the stratigraphic distribution of the most striking tractive facies indicates that there is also a relation between the enhancement of bottom current activity and the major perturbations of the global carbon cycle. Nd isotope data from Northern Tethyan localities indicate that circulation pattern in Atlantic-Tethys changed in consequence of the perturbation of the global carbon cycle at the beginning of OAE 2 [*Zheng et al.,* 2016]. We underline that SP2 is exclusive of the Pialli Level at Le Brecce and Monte Petrano sections (see supporting information S1). In particular, the upper part of the SP2 (Figure 7b), consisting of limestones with wavy and pervasive plane-parallel laminations (C2 and D2 facies), highlights strong bottom current reworking that appears to terminate the deposition of carbonate-poor homogeneous black shales.

In all the studied sections of the Umbria-Marche Basin, in the stratigraphic interval between the MCE I and the OAE 2, phases of enhanced bottom circulation are documented by the stacking of B2, C2, and D2 facies within the SP3a and SP3b (Figure 7c). This suggests that in the late Cenomanian, tractive bottom currents temporarily and repeatedly reoxygenated the seafloor during episodes of higher fertility and enhanced silica production or under an oligotrophic regime favoring calcareous plankton.

Indication of renewed bottom current activity after the OAE 2 is provided by the peculiar facies association above the Bonarelli Level (SP4, Figure 7d) mostly in the Umbria-Marche Basin (supporting information S1, Figures 10 and 11). Evidence of very low sediment accumulation/sediment removal, associated to hiatuses and condensation, is hence provided by the sediments immediately covering the Bonarelli Level, followed by a facies association documenting evidence of the plausibly most intense and long-lasting period of

bottom current activity through the studied interval. An increase in current intensity would produce a large amount of sediment drifts that are frequently subjected to slumping and instability [*Laberg and Camerlenghi*, 2008]. In particular, when sediments are rich in siliceous organisms, as in the studied interval above the Bonarelli Level, the intergranular contacts prevent consolidation, favoring sediment instability and erosion [*Volpi et al.,* 2003; *Laberg and Camerlenghi*, 2008]. The lithologic contrast at the top of the Bonarelli Level between black shales and radiolarian-rich layers and the overlaying limestones could act di per se both as a preferential boundary for erosion of unconsolidated sediments and as the basal surface for decollement and subsequent sediment deformation under shear stress. Hence, we presume that an increase in bottom current reworking soon after the Bonarelli event would have led to accumulation of vast drifted deposits easily subjected to syndepositional to slightly postdepositional deformation and even to slumping along slopes of the deepest part of the basin. This point deserves more studies of Tethyan and other pelagic basins to overcome the very little information still existing on the physiographic setting of the basins, drifts, soft-sediment deformation, and slumping in the Cretaceous oceans.

5.3. Bottom Water Circulation: Causal Links to Repetitive and/or Exceptional Climate Changes?

Hiatuses associated with OAEs are frequently described in both pelagic and coastal settings [e.g., *Föllmi et al.,* 1994; *Jones et al.,* 1994; *Drzewiecki and Simo*, 1997; *Weissert et al.,* 1998; *McArthur et al.,* 2000; *Jones and Jenkyns,* 2001; *Meyers and Sageman*, 2004; *Erbacher et al.,* 2005; *Robinson et al.,* 2008; *El-Sabbagh et al.,* 2011; *Caswell and Coe,* 2012] and explained as the result of changing current intensity along shelves and/or linked to general regressive trend in sea level [e.g., *Jaillard and Arnaud-Vanneau*, 1993; *Gröcke et al.,* 2006]. Recently, isotopic data [*Gambacorta et al.,* 2015] clearly documented major hiatuses of different duration (between 160 and 510 kyr) eliding the late part of the OAE 2 C isotopic anomaly and the interval immediately postdating the Bonarelli Level in all the studied sequences. The sedimentological evidence of intense winnowing and the isotopic data provide insight into the processes producing erosion and redistribution of bottom sediments during the latest phase of the OAE 2 and the following earliest Turonian time interval.

In several sections in the Anglo-Paris Basin, Bohemian-Saxonian Basin and the Western Interior Basin hiatuses have been documented at the onset of OAE 2 [*Voigt et al.,* 2006; *Jarvis et al.,* 2011; *Du Vivier et al.,* 2014; *Eldrett et al.,* 2015a). In particular, at the Pueblo reference section, a 60–100 kyr long missing time was estimated [see *Eldrett et al.*, 2015a]. A possible hiatus at the base of the Bonarelli Level was postulated by *Gambacorta et al.* [2015]. Although the $\delta^{13}C_{carb}$ and $\delta^{13}C_{org}$ records do not provide direct evidence of hiatuses at the onset of the OAE 2 isotopic anomaly, correlating with the Black Marker below the Bonarelli Level, the sharp lithologic boundary between limestone and black shale as well as in nitrogen and iron isotopes across the base of the Bonarelli Level [*Gambacorta et al.,* 2015] might suggest the presence of short hiatal interval.

Bottom currents operating in the modern and ancient oceans [*Rebesco and Stow*, 2001; *Knutz*, 2008; *Shanmugam*, 2008; *Gambacorta et al.,* 2014] clearly indicate that high flow velocities capable of winnowing and redistributing sediments do exist. Thermohaline-induced geostrophic bottom currents show a wide range of speeds with velocities usually ranging from 1 to 20 cm/s [*Hollister and Heezen*, 1972], but exceptionally faster currents have been observed in many areas of the present-day oceans with velocities reaching values up to 300 cm/s [*Shanmungam,* 2006 Wind-driven bottom currents such as the Loop Current in the eastern Gulf of Mexico [*Shanmungam,* 2006] can reach velocities of 25 cm/s at 500 m depth [*Nowlin and Hubert*, 1972] and 19 cm/s at a depth of 3286 m [*Pequegnat*, 1972].

In modern oceans, during the so-called benthic storms, bottom currents are subjected to periodical phases of intensification of the mean flow from 2 to 5 times faster than normal current velocities, and in some cases flow velocities of over 20 cm/s could be observed, with a very high concentration of suspended matter (up to 5 g L^{-1}) and a large erosional capability [*Hernández-Molina et al.,* 2008]. Such high-velocity currents surely play an important role in the redistribution of sediments at the seafloor [*Hollister et al.,* 1980; *Nowell and Hollister*, 1985; *Hollister*, 1993; *Hernández-Molina et al.,* 2008]. Indeed, benthic storms have enough velocity to resuspend sediments, produce sedimentary structures at the sediment/water interface, and rework sediments down to a depth of around 0.5 m [*Kennett*, 1982; *Bearmon*, 1989; *Hernández-Molina et al.,* 2008].

Internal waves, first reported by *Ekman* [1904], called also baroclinic currents, are another process able to develop high horizontal current velocities up to 2 m/s and vertical velocities of 20 cm/s [*Brandt et al.,* 2002; *Shanmugam*, 2008]. Seismic data from the Danish Basin show the presence of contourite drifts, moats, and

channels in the Upper Cretaceous chalk, with architectures similar to modern contourite systems of continental margins [*Surlyk and Lykke-Andersen*, 2007]. The observed seafloor relief is interpreted to have formed in a "chalk sea" in response to persistent bottom currents, flowing parallel to bathymetric contours. At last, in order to explain the frequent erosions observed at the base of the Paleozoic black shales, *Baird and Brett* [1986, 1991] and *Baird et al*. [1988] suggested the action of deep storm waves, density currents, and internal waves connected to the existence of a vertical chemical stratification of the water column.

Based on the recurrent gap and facies association at the top of the Bonarelli Level, we speculate that in Umbria-Marche and Belluno Basins OAE 2 terminated with a phase of very effective bottom currents producing erosion, winnowing and in a few cases soft-sediment deformation, concurrent with reventilation of the seafloor. It is possible that these processes occurred at a wider scale, because evidence of ocean current intensification during OAE 2 along the Northern Tethys was also described by *Wohlwend et al.* [2015]. These authors interpreted sedimentary gaps combined with prominent glauconite quartz sandstones as the result of intense erosive east-west trending shelf currents.

During OAE 2 the oceans went through a time of extremely high temperatures, and the consequent reduced latitudinal thermal gradients [*Huber et al.,* 1995; *Skelton et al.,* 2003; *Donnadieu et al.,* 2006; *Hay*, 2008] must have strongly affected the formation of deep waters as driver of thermohaline circulation. Nd isotope data measured across OAE 2 provide evidence for an enhanced deep water transfer from Tethys toward the Atlantic [*Martin et al.,* 2012]. The source of this deep water may have been located on the carbonate shelves of the southern Tethys [*Martin et al.,* 2012] and/or on the vast Arabian carbonate platform in the eastern Tethys.

During the recovery from OAE 2 conditions, the decrease in atmospheric greenhouse gases might have induced the progressive reestablishment of the latitudinal thermal gradient. Once high-latitude cooling reached a critical threshold, thermohaline bottom current circulation could have caused oceanic overturning, reoxygenating the deep ocean, and inducing the rapid reestablishment of preperturbation conditions. The detailed chronology of paleotemperature trends in the Cenomanian-Turonian interval [e.g., *Jarvis et al.,* 2011], however, indicates that the Cretaceous thermal maximum was reached in earliest Turonian time, shortly but unambiguously after termination of OAE 2, and that cooling started at younger stages. Consequently, we believe that the scenario described above cannot be applied to explain the end of global anoxia in the Cenomanian/Turonian boundary interval.

Cretaceous ocean circulation was modeled by *Hay* [2008, 2009] who envisioned heat transfer via mesoscale eddies and absence of a global thermohaline circulation. In an eddy-dominated ocean, replenishment of oxygen in deep waters is extremely difficult, especially because the globally warm surface waters would have been oxygen poor to start with: Dysoxia-anoxia was then easy to reach and difficult to switch off at global scale. The Cretaceous was also characterized by vast epeiric seas with complex individual bathymetry: Deep water formation, circulation, and oxygenation were most probably linked to individual basins other than global patterns [*Hay,* 2008, 2009].

Under Mid-Cretaceous greenhouse conditions [*Jenkyns*, 2010; *Pagani et al.,* 2014, and references therein] oceanic circulation might have been controlled by warm saline bottom waters originated in epicontinental tropical seas as proposed by *Brass et al.* [1982], following the original ideas of *Chamberlin* [1906] who postulated a reversal (relative to today flows) in deep sea circulation under excess greenhouse gases and climate warming. *Brass et al.* [1982] incorporated this scenario into the "warm saline bottom water (WSBW)" hypothesis for the Mid-Cretaceous ocean where thermohaline circulation resulted from sinking of very warm brines in the tropics instead of cold and relatively salty waters today downwelling at high latitudes. Under greenhouse climate, increased evaporation in tropical shelf areas formed warm saline waters that, thus, became deep currents at low latitudes and transported heat poleward.

Friedrich et al. [2008] based on oxygen isotopes and Mg/Ca ratios from benthic foraminifera at Demarara Rise in the equatorial Atlantic Ocean, supported the WSBW hypothesis. They reconstructed paleotemperatures of 20–25°C for intermediate waters with very high salinity that determined dysoxic-anoxic conditions in the tropical proto-Atlantic during the late Cenomanian. Specifically, in the interval bracketed by the MCE I and OAE 2 repetitive local production of warm deep brines disrupted ocean stratification and the oxygen minimum zone affecting the renewal of deep waters in the proto-Atlantic Ocean [*Friedrich et al.,* 2008].

In Figure 10 the evolution of the SP in the latest Albian to earliest Turonian studied interval and the inferred bottom current intensities are compared to the simplified $\delta^{18}O$ record of *Friedrich et al.* [2008]. We underline that the sharp increase in bottom current activity recorded by SP in the Scaglia Bianca at the onset of the MCE I and persisting up to the OAE 2 is coeval with the interval of high salinity intermediate waters at Demerara Rise [*Friedrich et al.,* 2008]. Our record points to the recurrence of dense and active bottom currents at intermediate depth and suggests that warm saline deep waters were possibly not only restricted to the tropical Atlantic Ocean but also existed in the western Tethys. Our detailed record of the Umbria-Marche Basin (see supporting information S1) further indicates that before the deposition of the Bonarelli Level tractive structures, postdating individual rhythmic black shales were presumably induced by recurrent dense bottom water flows, which terminated intermittent dysoxic-anoxic conditions. We believe that the repetitive late Cenomanian black layers represent short-lived episodes of anoxia due to stratification of water masses, similarly to late Albian black shales [e.g., *Tiraboschi et al.,* 2009]. In fact, although some expansion of the oxygen minimum zone cannot be ruled out, we believe that the paleowater depth and the pelagic setting of the studied sections concur in minimizing, if not excluding, the interaction of the base of the oxygen minimum zone with the sediment/water interface.

Since the black shale-black chert layers of late Cenomanian age were proven to be controlled by Milankovitch cycles [*Mitchell et al.,* 2008; *Lanci et al.,* 2010], then also bottom current activity might have been regulated astronomically. This is in agreement with recent documentation by *Eldrett et al.* [2015b] of Milankovitch cyclicity in recurrent activity and break down of stratification in the Western Interior Basin.

Intermittent delivery of shelf brines to intermediate deep waters in the proto-Atlantic was postulated by *Voigt* [2008] to reconcile general oxygen depletion and the $\delta^{18}O$ record at Demerara Rise [*Friedrich et al.,* 2008]. Such brines were possibly dense enough to penetrate into the western Tethys, perhaps similarly to the extant Mediterranean outflow affecting the Atlantic away from the Gibraltar Strait and leaving imprints of sediment reworking and erosion along the European margin [*Hernández-Molina et al.,* 2014], or the brines originated in the western Tethys, as suggested by Nd isotope data [*Martin et al.,* 2012] and then penetrated into the Atlantic Ocean.

Within the Bonarelli Level the occurrence of black shales and radiolarian layers suggests varying mesotrophic to eutrophic conditions in surface waters and possible shallowing of the CCD. Bottom current activity is difficult to depict from sedimentological observation (Figure 6), but discrete radiolarian layers might derive from winnowing of the seafloor and therefore might correspond to times of relatively active bottom currents. A cooling event has been documented and dated within OAE 2 [*Jarvis et al.,* 2011; *Eldrett et al.,* 2014; *Van Helmond et al.,* 2016]: The "Plenus Cold Event" was associated to a drop in paleo-CO_2 concentration [*Barclay et al.,* 2010], interrupted globally warm conditions, favored the north to south migration of boreal taxa, and locally triggered benthic foraminiferal repopulation events [*Friedrich et al.,* 2011]. In the studied sections, radiolarian layers dominate over black shales in the lowermost part of the Bonarelli Level, below the level corresponding to peak "a" of the $\delta^{13}C$ anomaly [*Gambacorta et al.,* 2015]. The initial phase of OAE 2 was globally marked by a major warming [e.g., *Forster et al.,* 2007] that might have favored the formation of warm salty waters along tropical margins in the Atlantic and Tethys Oceans. Possibly, this was the onset of enhanced WSBW that produced local hiatuses and winnowing at the seafloor. The Plenus Cold Event interrupted formation of dense saline water masses and favored the deposition of black shales in the Umbria-Marche Basin. The upper part of the Bonarelli Level, correlatable to peak "b" of the $\delta^{13}C$ anomaly [*Gambacorta et al.,* 2015], is characterized by alternating radiolarian layers and black shales chert (Figure 6), suggesting the reactivation of intermittent effective bottom currents under greenhouse conditions.

Indeed, *Friedrich et al.* [2008] showed that in the equatorial Atlantic Ocean a younger phase of warm salty intermediate waters correlates with the late part of the OAE 2 C isotope anomaly and the immediately following interval. Although the sections studied in the Umbria-Marche and Belluno Basins are affected by hiatuses in the OAE 2 interval, we emphasize the correlation between most intense bottom currents and the hypothesized formation of saline intermediate waters in the Tethys (Figures 10 and 11). In particular, the most intense bottom currents coincide with the gap occurring in the lowermost Turonian interval (Figures 10 and 11) immediately at the top of the Bonarelli Level, as it has been discussed in section 5.2. Indeed, as illustrated in Figures 10 and 11, the earliest Turonian thermal maximum (between the end of OAE 2 and the Tu1 event) [*Jarvis et al.,* 2011] might have induced the development of saline waters along

Tethyan shelves and then entered in the proto-Atlantic. Alternatively or concomitantly warm saline waters might have formed in the tropical Atlantic, affecting intermediate and deep circulation also in Tethyan basins. Such dense flows might have caused major reworking/displacement/erosion of sediments on the seafloor during the initial phase of recovery from anoxic conditions with elision of the first oxic sediments on top of the Bonarelli Level and part of the underlying black shales, corresponding to a 160–510 kyr long record [*Gambacorta et al.,* 2015] (Figures 7d).

As it has been discussed, the Ha-b–E2 facies association (Figure 7d) in the lower part of the Tu 1–Tu 2 interval, postdating the hiatus (Figure 11), derives from strong current reworking of the seafloor. We suggest that after the stage of most intense current activity, resulting in the erosion of sediments, the decrease of bottom current shear stress promoted deposition of the E2 facies, as it is testified by the foraminiferal lags in the upper part of the Tu 1–Tu 2 interval. In all the studied sections, foraminiferal lags are restricted to this interval and might derive from bottom waters formed during the early Turonian cooling presumably inducing downwelling of cooler and denser water masses. Indeed, such structures were not observed during times of greenhouse conditions in the late Albian-earliest Turonian interval.

A marked drop in bottom current activity correlates with the uppermost Scaglia Bianca limestone, possibly corresponding to the onset of a very different regime without evidence of sediment winnowing or displacement.

Geological data indicate that the OAE 1d correlates with higher paleotemperatures [*Wilson and Norris*, 2001] and intensified bottom currents (this study, see supporting information S1). Similarly to the interval between the MCE I and OAE 2, we suggest that the black shales of the OAE 1d (Pialli Level) might result from intermittent water stratification disrupted by intense bottom currents. The exclusive presence of SP2 might suggest that eutrophic conditions were never reached and perhaps that WSBW was not operating. Black shales of the Pialli Level are very similar to those documented in the upper Albian in the Umbria-Marche Basin [*Herbert and Fischer*, 1986; *Premoli Silva et al.,* 1989; *Erba*, 1992; *Galeotti et al.,* 2003] and interpreted as the result of recurrent stratification due to enhanced precipitation and freshwater runoff forming a pycnocline that reduced deep water renewal and bottom oxygenation [*Tiraboschi et al.,* 2009].

In the studied sections, and, in general, in the Umbria-Marche and Belluno Basins, periods of low intensity of bottom currents correspond to a color shift from light grey/whitish calcilutites/marlstones to reddish hematite-rich micritic limestones/marlstones above both the Bonarelli Level and the post-OAE 1d Pialli Level (Figures 2, 3, and 10). This confirms a change in clay input and a general increase in oxygenation of bottom waters, during periods of mild bottom circulation [*Xi et al.,* 2007; *Hu et al.,* 2009; *Neuhuber and Wagreich*, 2011; *Wang et al.,* 2011], originated at temperate source areas with downwelling of cooler waters.

6. Conclusions

The data set from the latest Albian–lower Turonian pelagic successions of the Umbria-Marche and Belluno Basins suggests that a dynamic circulation affected the seafloor in western Tethys. Depositional patterns suggest a strong interplay of oceanographic changes in surface waters as well as in the intensity of bottom currents, during OAE 1d, MCE I and OAE 2, and the interludes between them. The coupling of surface and bottom water processes determined the establishment and recovery from environmental perturbations, with different modalities through the latest Albian–early Turonian.

Under oxygenated bottom waters, the switch from an oligotrophic to an eutrophic state of surface waters controlled the shift from calcareous to siliceous deposition. At sites and times of anoxia, siliceous and organic-rich shales (black shales) replace each other as a function of the trophic level: Black shales correspond to oligotrophic-mesotrophic/eutrophic and black cherts exclusively to eutrophic conditions. Moreover, shale layers possibly represent the lowest sedimentation rates (condensation), after substantial reduction of the carbonate component (low productivity), and of the siliceous components (high dissolution).

High-resolution biochemostratigraphy allows dating SP types that result to be largely repetitive and recurrent at different time scales. The association of the observed facies shows the recurrence of four major SP types, all of them including indications of bottom current activity. Invariably, the position of tractive facies within the SPs indicates that they were responsible of the termination of intermittent or prolonged anoxia. This systematic association documents the role of bottom currents in the recovery to normal environmental conditions.

As phases of enhanced bottom circulation represent repetitive events, the identified rhythmicity has various orders of magnitude, ranging from the meter scale expressed by the four described SP types to the millimeter scale evidenced by the internal variations observed in the black shale and bedded black chert facies (G4a).

Evidence of traction-related facies immediately following OAE 1d and OAE 2 suggests that the times of most intense circulation ("extraordinary reventilation events") postdated the major perturbations of the global carbon cycle. These phases of intensified ventilation must have played an important role in reestablishing normal water masses trophism and oxygenation. Intense sea bottom currents had important effects on sediment redistribution causing the widely observed erosional gap at the top of the Bonarelli Level.

Our study documents a systematic termination of dysoxic-anoxic conditions at times of intense bottom currents that renewed oxygen at the seafloor while eroding/displacing accumulated particles. Climate changes were influential on deep circulation dynamics. Under late Cenomanian-earliest Turonian greenhouse conditions, vigorous bottom currents were arguably induced by warm, dense saline intermediate to deep waters originated in tropical shelves, perhaps entering the western Tethys from the central Atlantic Ocean, or originated in tropical shelf areas within the Tethys Ocean Evidence of effective bottom currents characterize the interval immediately preceding and marking the onset of OAE 2, associated to the initial phase of major global warming. Within the Bonarelli Level, radiolarian layers in the lower part correlate with warm condition, while black shale dominates in the stratigraphic interval corresponding to the Plenus Cold Event around the $\delta^{13}C$ peak a. In the upper part of the Bonarelli Level, alternating radiolarian layers and black shales chert suggest the revival of intermittent active bottom currents under greenhouse conditions. The hiatuses detected at the top of the Bonarelli Level, interpreted as the result of erosion caused by the most effective bottom currents, correspond to the early Turonian thermal maximum.

Tractive facies postdating intermittent anoxia during OAE 1d and in the interval bracketed by MCE I and OAE 2 are indicative of more efficient bottom currents, though capable of disrupting stratification and replenish deep water with oxygen.

In the studied successions, in the upper Albian–lower Turonian interval, minimal (or absent) sediment displacement correlates with a color change to reddish lithologies of the pre- and post-OAE 1d interval and the Scaglia Rossa Formation (Figure 10). Although the paleotemperature reconstructions are still loose, reddish lithologies corresponding to times of relatively cooler conditions [i.e., *Wang et al.*, 2011] might indicate a mechanism of deep water formation different from saline waters at low-latitude characteristic of warm climatic conditions. Possibly, during times of decreasing temperature after warming episodes, cooler oxygen-richer bottom water masses originated at higher latitudes.

Appendix A

Supplementary data associated with this article include the Furlo, Contessa, Le Brecce, Monte Petrano (lower and upper part), and Cismon (lower and upper part) composite sections.

Acknowledgments

We acknowledge Hugh Jenkyns and Isabella Premoli Silva for passionate discussion and for sharing ideas. The paper definitely benefited from the constructive reviews of the Associate Editor, as well as from thoughtful criticisms by James Eldrett and Michael Wagreich. The research was conducted within the MIUR-PRIN2011 (2010X3PP8J) awarded to E.E. Data presented in the paper can be accessed by contacting the corresponding author at gabriele.gambacorta@guest.unimi.it.

References

Alvarez, W. (1990), Pattern of extensional faulting in pelagic carbonates of the Umbria-Marche Apennines of central Italy, *Geology*, *18*, 407–410.

Arthur, M. A., and I. Premoli Silva (1982), Development of widespread organic carbon-rich strata in the Mediterranean Tethys, in *Nature and Origin of Cretaceous Carbon-Rich Facies*, edited by S. O. Schlanger and M. B. Cita, pp. 7–54, Academic Press, London, U. K.

Arthur, M. A., H.-J. Brumsack, H. C. Jenkyns, and S. O. Schlanger (1990), Stratigraphy, geochemistry, and paleoceanography of organic carbon-rich Cretaceous sequences, in *Cretaceous Resources Events, and Rhythms*, edited by R. Ginsburg and B. Beaudoin, pp. 75–119, Kluwer Acad. Press, Netherlands.

Baird, G. C., and C. E. Brett (1986), Erosion on an anaerobic seafloor: Significance of reworked pyrite deposits from the Devonian of New York State, *Palaeogeogr. Palaeoclimatol. Palaeoecol.*, *57*, 157–193.

Baird, G. C., and C. E. Brett (1991), Submarine erosion on the anoxic seafloor: Stratinomic paleoenvironmental, and temporal significance of reworked pyrite-bone beds, in *Modern and Ancient Shelf Anoxia*, edited by R. V. Tyson and T. H. Pearson, *Geol. Soc. London Spec. Publ.*, *58*, 233–257.

Baird, G. C., C. E. Brety, and W. T. Kirchgasser (1988), Genesis of black shale-roofed discontinuities in the Genesee Formation, western New York State, in *Devonian of the World*, *Memoir*, vol. 14, edited by N. J. McMillan, A. F. Embry, and D. J. Glass, pp. 357–375, Can. Soc. Pet. Geol., Calgary, Canada.

Barclay, R. S., J. C. McElwain, and B. B. Sageman (2010), Carbon sequestration activated by a volcanic CO2 pulse during Ocean Anoxic Event 2, *Nat. Geosci.*, *3*, 205–208, doi:10.1038/NGEO757.

Bearmon, G. (1989), *Ocean Chemistry and Deep-Sea Sediments*, Open Univ., Oceanogr. Course Team, Pergamon Press, London, U. K.

Beaudoin, B., E. P. M'Ban, A. Montanari, and M. Pinault (1996), Lithostratigraphie haute résolution (<20 ka) dans le Cénomanien du bassin d'Ombrie-Marches (Italie), in *Comptes Rendus de l'Académie des Sciences Paris*, *Series Iia*, vol. 323, pp. 689–696, Paris, France.
Bellanca, A., M. Claps, E. Erba, D. Masetti, R. Neri, I. Premoli Silva, and F. Venezia (1996), Orbitally induced limestone/marlstone rhythms in the Albian-Cenomanian Cismon section (Venetian region, Northern Italy): Sedimentology, calcareous and siliceous plankton distribution, elemental and isotope geochemistry, *Palaeogeogr. Palaeoclimatol. Palaeoecol.*, *126*, 227–260.
Bernoulli, D., and H. C. Jenkyns (1974), Alpine, Mediterranean, and Central Atlantic Mesozoic facies in relation to the early evolution of the Tethys, in *Modern and Ancient Geosynclinal Sedimentation*, *Spec. Publ.*, vol. 19, edited by R. H. Dott and R. H. Shaver, pp. 129–160, Soc. Econ. Paleontologists Mineralogists, Tulsa, Okla.
Bonarelli, G. (1891), Il territorio di Gubbio: Notizie geologiche, in *Tipografia Economica*, 38 pp., Roma.
Bosellini, A., C. Broglio Loriga, and C. Busetto (1978), I bacini cretacei del Trentino, *Riv. Ital Paleont. Strat*, *84*(4), 897–946.
Bralower, T. J., R. M. Leckie, W. V. Sliter, and H. R. Thierstein (1995), An integrated Cretaceous timescale, in *Geochronology Time Scales and Global Stratigraphic Correlation*, *Spec. Publ.*, vol. 54, edited by W. A. Berggren et al., pp. 65–79, SEPM, Tulsa, Okla.
Brandt, P., A. Rubino, and J. Fischer (2002), Large-amplitude internal solitary waves in the North Equatorial Countercurrent, *J. Phys. Oceanogr.*, *32*, 1567–1573.
Brass, G. W., J. R. Southam, and W. H. Peterson (1982), Warm saline bottom water in the ancient ocean, *Nature*, *296*, 620–623.
Brumsack, H.-J. (2006), The trace metal content of recent organic carbon-rich sediments: Implications for Cretaceous black shale formation, *Palaeogeogr. Palaeoclimatol. Palaeoecol.*, *232*, 344–361.
Burnett, J. A. (1998), Upper Cretaceous, in *Calcareous Nannofossil Biostratigraphy*, edited by P. R. Bown, pp. 132–199, Chapman and Hall, London.
Caswell, B. A., and A. L. Coe (2012), A high-resolution shallow marine record of the Toarcian (Early Jurassic) oceanic anoxic event from the East Midlands Shelf, UK, *Palaeogeogr. Palaeoclimatol. Palaeoecol.*, *365–6*, 124–135.
Chamberlin, T. C. (1906), On a possible reversal of deep-sea circulation and its influence on geologic climates, *J. Geol.*, *14*, 363–373.
Channell, J. E. T., B. D'Argenio, and F. Horvath (1979a), The African promontory, in *Mesozoic Mediterranean Paleogeography*, *Earth Sci. Rev.*, vol. 15, pp. 213–272, Elsevier, Amsterdam.
Channell, J. E. T., W. Lowrie, and F. Medizza (1979b), Middle and Early Cretaceous magnetic stratigraphy from the Cismon section, Northern Italy, *Earth Planet. Sci. Lett.*, *42*(2), 153–166.
Claps, M., and D. Masetti (1994), Milankovitch periodicities recorded in Cretaceous deep-sea sequences from the Southern Alps (Northern Italy), *Spec. Publ. Int. Assoc. Sediment.*, *19*, 99–107.
Claps, M., D. Masetti, F. Pedrielli, and A. Garavello (1991), Analisi spettrale e cicli di Milankovitch in successioni cretaciche del Sudalpino orientale, *Riv. Ital. Paleontol. Stratigr.*, *97*, 153–174.
Coccioni, R., and S. Galeotti (2001), The mid-Cenomanian event the prelude to the OAE 2, *EOS Trans. AGU 82(47)*, Fall Meet. Suppl.
Coccioni, R., and S. Galeotti (2003), The mid-Cenomanian event: Prelude to OAE 2, *Palaeogeogr. Palaeoclimatol. Palaeoecol.*, *190*, 427–440.
Coccioni, R., S. Galeotti, and D. Ragni (1992), Litho- and biostratigraphy of the Scaglia Bianca Formation (late Albian-late Cenomanian) in the Umbria-Marche Apennines (Italy), paper presented at the *6th Annual Meeting of IGCP 262* (*Tethyan Cretaceous Correlation*) "*Cretaceous Facies in Orogenic Belts*", Athens, 22–26 May, 1992, p. 4.
Dercourt, J., M. Gaetani, B. Vrielinck, E. Barrier, B. Biju-Duval, M. F. Brunet, J. P. Cadet, S. Crasquin, and M. Sandulescu (Eds) (2000), *Atlas of Peri-Tethys, Palaeogeographical Maps*, Commission de la Carte Geologique du Monde (CCGN/CGMW), Paris, France.
Donnadieu, Y., R. Pierrehumbert, R. Jacob, and F. Fluteau (2006), Modelling the primary control of paleogeography on Cretaceous climate, *Earth Planet. Sci. Lett.*, *248*, 426–437.
Drzewiecki, P. A., and J. A. Simo (1997), Carbonate platform drowning and oceanic anoxic events on a Mid-Cretaceous carbonate platform, south-central Pyrenees, Spain, *J. Sediment. Res.*, *67*, 698–714.
Du Vivier, A. D. C., D. Selby, B. B. Sageman, I. Jarvis, D. R. Gröcke, and S. Voigt (2014), Marine $^{187}Os/^{188}Os$ isotope stratigraphy reveals the interaction of volcanism and ocean circulation during oceanic anoxic event, *Earth Planet. Sci. Lett.*, *389*, 23–33.
Ekman, V. W. (1904), On dead water, in *Norwegian North Polar Expedition 1893–1896*, *Scientific Results*, vol. 5, edited by F. Nansen, Christiania J. Bybwad, London.
Eldrett, J. S., D. Minisini, and S. C. Bergman (2014), Decoupling of the carbon cycle during Ocean Anoxic Event 2, *Geology*, doi:10.1130/G35520.1.
Eldrett, J. S., C. Ma, S. C. Bergman, A. Ozkan, D. Minisini, B. Lutz, S.-J. Jackett, C. Macaulay, and A. E. Kelly (2015a), Origin of limestone–marlstone cycles: Astronomic forcing of organic-rich sedimentary rocks from the Cenomanian to early Coniacian of the Cretaceous Western Interior Seaway, USA, *Earth Planet. Sci. Lett.*, *423*, 98–113.
Eldrett, J. S., et al. (2015b), An astronomically calibrated stratigraphy of the Cenomanian, Turonian and earliest Coniacian from the Cretaceous Western Interior Seaway, USA: Implications for global chronostratigraphy, *Cretaceous Res.*, *56*, 316–344.
El-Sabbagh, A., A. A. Tantawy, G. Keller, H. Khozyem, J. Spangenberg, T. Adatte, and B. Gertsch (2011), Stratigraphy of the Cenomanian-Turonian oceanic anoxic vent OAE2 in shallow shelf sequences of NE Egypt, *Cretaceous Res.*, *32*, 705–722.
Erba, E. (1992), Calcareous nannofossil distribution in pelagic rhythmic sediments (Aptian-Albian Piobbico core, central Italy), *Riv. Ital. Paleontol. Stratigr.*, *97*, 455–484.
Erba, E. (2004), Calcareous nannofossils and Mesozoic oceanic anoxic events, *Mar. Micropaleontol.*, *52*, 85–106.
Erba, E. (2006), The first 150 million years history of calcareous nannoplankton: Biosphere–geosphere interactions, *Palaeogeogr. Palaeoclimatol. Palaeoecol.*, *232*, 237–250.
Erba, E., and R. L. Larson (1998), The Cismon APTICORE (Southern Alps, Italy): A reference section for the Lower Cretaceous at low latitudes, *Riv. Ital. Paleontol. Stratigr.*, *104*, 181–192.
Erba, E., and F. Tremolada (2004), Nannofossil carbonate fluxes during the Early Cretaceous: Phytoplankton response to nitrification episodes, atmospheric CO_2 and anoxia, *Paleoceanography*, *19*, PA1008, doi:10.1029/2003PA000884.
Erbacher, J., O. Friedrich, P. A. Wilson, H. Birch, and J. Mutterlose (2005), Stable organic carbon isotope stratigraphy across oceanic anoxic event 2 of Demerara Rise, western tropical Atlantic, *Geochem. Geophys. Geosyst.*, *6*, Q06010, doi:10.1029/2004GC000850.
Föllmi, K. B., H. Weissert, M. Bisping, and H. Funk (1994), Phosphogeneis, carbon-isotope stratigraphy, and carbonate-platform evolution along the Lower Cretaceous northern Tethyan margin, *Geol. Soc. Am. Bull.*, *106*, 729–746.
Forster, A., S. Schouten, K. Moriya, P. A. Wilson, and J. S. Sinninghe Damsté (2007), Tropical warming and intermittent cooling during the Cenomanian/Turonian oceanic anoxic event 2: Sea surface temperature records from the equatorial Atlantic, *Paleoceanography*, *22*, PA1217, doi:10.1029/2006PA001349.
Friedrich, O., J. Erbacher, K. Moriya, P. A. Wilson, and H. Kuhnert (2008), Warm saline intermediate waters in the Cretaceous tropical Atlantic Ocean, *Nat. Geosci.*, *1*, 453–457.

Friedrich, O., J. Erbacher, P. A. Wilson, K. Moriya, and J. Mutterlose (2009), Paleoenvironmental changes across the mid Cenomanian event in the tropical Atlantic Ocean (Demerara Rise, ODP Leg 207) inferred from benthic foraminiferal assemblages, *Mar. Micropaleontol.*, *71*, 28–40.

Friedrich, O., S. Voigt, T. Kuhnt, and M. C. Koch (2011), Repeated bottom-water oxygenation during OAE 2: Timing and duration of short-lived benthic foraminiferal repopulation events (Wunstorf, northern Germany), *J. Micropalaeontol.*, *30*, 119–128.

Galeotti, S., M. Sprovieni, R. Coccioni, A. Bellanca, and R. Neri (2003), Orbitally modulated black shale deposition in the upper Albian Amadeus Segment (central Italy): A multi-proxy reconstruction, *Palaeogeogr. Palaeoclimatol. Palaeoecol.*, *190*, 441–458.

Gambacorta, G., R. Bersezio, and E. Erba (2014), Sedimentation in the Tethyan pelagic realm during the Cenomanian: Monotonous settling or active redistribution?, *Palaeogeogr. Palaeoclimatol. Palaeoecol.*, *409*, 301–319.

Gambacorta, G., H. C. Jenkyns, F. Russo, H. Tsikos, P. Wilson, G. Faucher, and E. Erba (2015), Carbon- and oxygen-isotope records of Mid-Cretaceous Tethyan pelagic sequences from the Umbria–Marche and Belluno Basins (Italy), *Newsl. Stratigr.*, *48*(3), 299–323.

Giorgioni, M., H. Weissert, S. M. Bernasconi, P. A. Hochuli, R. Coccioni, and C. E. Keller (2012), Orbital control on carbon cycle and oceanography in the Mid-Cretaceous greenhouse, *Paleoceanography*, *27*, PA1204, doi:10.1029/2011PA002163.

Giorgioni, M., H. Weissert, S. M. Bernasconi, P. A. Hochuli, C. E. Keller, R. Coccioni, M. R. Petrizzo, A. Lukeneder, and T. I. Garcia (2015), Paleoceanographic changes during the Albian–Cenomanian in the Tethys and North Atlantic and the onset of the Cretaceous chalk, *Global Planet. Change*, *126*, 46–61.

Gröcke, D. R., G. A. Ludvigson, B. L. Witzke, S. L. Robinson, R. M. Joeckel, D. F. Ufnar, and R. L. Ravn (2006), Recognizing the Albian-Cenomanian (OAE1d) sequence boundary using plant carbon isotopes: Dakota Formation, Western Interior Basin, USA, *Geology*, *34*, 193–196.

Hay, W. W. (2008), Evolving ideas about the Cretaceous climate and ocean circulation, *Cretaceous Res.*, *29*, 725–753.

Hay, W. W. (2009), Cretaceous oceans and ocean modeling, in *Cretaceous Oceanic Red Beds: Stratigraphy, Composition, Origins, Paleoceanographic, and Paleoclimatic Significance*, *Spec. Publ.*, vol. 91, edited by X. M. Hu et al., pp. 137–145, SEPM, Tulsa, Okla.

Herbert, T. D., and A. G. Fischer (1986), Milankovitch climatic origin of Mid-Cretaceous black shale rhythms in central Italy, *Nature*, *329*, 739–743.

Hernández-Molina, F. J., A. Maldonado, and D. A. V. Stow (2008), Abyssal plain controurites, in *Contourites*, *Dev. Sediment.*, vol. 60, edited by M. Rebesco and A. Camerlenghi, pp. 345–378, Elsevier, Amsterdam.

Hernández-Molina, F. J., et al. (2014), Onset of Mediterranean outflow into the North Atlantic, *Science*, *344*, 1244–1250.

Hollister, C. D. (1993), The concept of deep-sea contourites, *Sediment. Geol.*, *82*, 5–11.

Hollister, C. D., and B. C. Heezen (1972), Geologic effects of ocean bottom currents: Western North Atlantic, in *Studies in Physical Oceanography*, vol. 2, edited by A. L. Gordon, pp. 37–66, Gordon and Breach Sci. Publ., New York.

Hollister, C. D., A. R. M. Nowell, and J. D. Smith (1980), The Third Annual Report of the High Energy Boundary Layer Experiment, *WHOI. Tech. Rep.*, *80*, 32–48.

Hori, R. S., C. Cho, and H. Umeda (1993), Origin of cyclicity in Triassic-Jurassic radiolarian bedded cherts of the Mino accretionary complex from Japan, *Island Arc*, *3*, 170–180.

Horner-Devine, M. C., M. A. Leibold, V. H. Smith, and B. J. M. Bohannan (2003), Bacterial diversity patterns along a gradient of primary productivity, *Ecol. Lett.*, *6*, 613–622.

Hsü, K. J., and H. C. Jenkyns (Eds.) (1974), *Pelagic Sediments: On Land and Under the Sea*, *Spec. Publ.*, pp. 1–456, Blackwell Sci. Publ., Osney Mead, Oxford.

Hu, X., W. Cheng, and J. Ji (2009), Origin of Cretaceous oceanic red beds from the Vispi Quarry section, central Italy: Visible reflectance and inorganic geochemistry, in *Cretaceous Oceanic Red Beds: Stratigraphy, Composition, Origins, Paleoceanographic, and Paleoclimatic Significance*, *Spec. Publ.*, vol. 91, edited by X. Hu et al., pp. 183–197, SEPM, Tulsa, Okla.

Huber, B. T., D. A. Hodell, and C. P. Hamilton (1995), Middle–Late Cretaceous climate of the southern high latitudes: Stable isotopic evidence for minimal equator-to-pole thermal gradients, *Geol. Soc. Am. Bull.*, *107*, 1164–1191.

Hüneke, H., and T. Mulder (Eds.) (2011), Deep-sea Sediments, *Dev. Sedimentol.*, *63*, 1–750.

Jaillard, E., and A. Arnaud-Vanneau (1993), The Cenomanian-Turonian transition on the Peruvian margin, *Cretaceous Res.*, *14*, 585–605.

Jarvis, I., A. S. Gale, H. C. Jenkyns, and M. A. Pearce (2006), Secular variation in Late Cretaceous carbon isotopes: A new $\delta^{13}C$ carbonate reference curve for the Cenomanian–Campanian (99.6–70.6 Ma), *Geol. Mag.*, *143*, 561–608.

Jarvis, I., J. S. Lignum, D. R. Gröcke, H. C. Jenkyns, and M. A. Pearce (2011), Black shale deposition, atmospheric CO_2 drawdown, and cooling during the Cenomanian–Turonian oceanic anoxic event, *Paleoceanography*, *26*, PA3201, doi:10.1029/2010PA002081.

Jenkyns, H. C. (2010), Geochemistry of oceanic anoxic events, *Geochem. Geophys. Geosyst.*, *11*, Q03004, doi:10.1029/2009GC002788.

Jones, C. E., and H. C. Jenkyns (2001), Seawater strontium isotopes, oceanic anoxic events, and seafloor hydrothermal activity in the Jurassic and Cretaceous, *Am. J. Sci.*, *301*, 112–149.

Jones, C. E., H. C. Jenkyns, A. L. Coe, and S. P. Hesselbo (1994), Strontium isotopic variations in Jurassic and Cretaceous seawater, *Geochim. Cosmochim. Acta*, *58*, 3061–3074.

Kennett, J. P. (1982), The geologic record of bottom currents, in *Marine Geology*, edited by J. P. Kennett, pp. 505–534, Prentice-Hall, New York.

Knutz, P. C. (2008), Paleoceanographic significance of contourite drifts, in *Contourites*, *Dev. Sedimentol.*, vol. 60, edited by M. Rebesco and A. Camerlenghi, pp. 511–535, Elsevier, Amsterdam.

Laberg, J. S., and A. Camerlenghi (2008), The significance of contourites for submarine slope stability, in *Contourites*, *Dev. Sedimentol.*, vol. 60, edited by M. Rebesco and A. Camerlenghi, pp. 537–556, Elsevier, Amsterdam.

Lalli, C. M., and T. Parsons (Eds) (1997), *Biological Oceanography: An Introduction*, Open Univ., Oceanogr. Course Team, Pergamon Press, London, U. K.

Lanci, L., G. Muttoni, and E. Erba (2010), Astronomical tuning of the Cenomanian Scaglia Bianca Formation at Furlo, Italy, *Earth Planet. Sci. Lett.*, *292*, 231–237.

Leckie, R. M., T. J. Bralower, and R. Cashman (2002), Oceanic anoxic events and plankton evolution: Biotic response to tectonic forcing during the Mid-Cretaceous, *Paleoceanography*, *17*(3), 1041, 13–29, doi:10.1029/2001PA000623.

Margalef, R. (1978), Life forms of phytoplankton as survival alternatives in an unstable environment, *Oceanol. Acta*, *134*, 493–509.

Martin, E. E., K. G. MacLeod, A. Jiménez Berrocoso, and E. Bourbon (2012), Water mass circulation on Demerara Rise during the Late Cretaceous based on Nd isotopes, *Earth Planet. Sci. Lett.*, *327–328*, 111–120.

McArthur, J. M., D. T. Donovan, M. F. Thirlwall, B. W. Fouke, and D. Mattey (2000), Strontium isotope profile of the Early Toarcian (Jurassic) oceanic anoxic event, the duration of ammonite biozones, and belemnite palaeotemperatures, *Earth Planet. Sci. Lett.*, *179*, 269–285.

Meyers, S. R., and B. B. Sageman (2004), Detection, quantification, and significance of hiatuses in pelagic and hemipelagic strata, *Earth Planet. Sci. Lett.*, *224*, 55–72.

Mitchell, R. N., D. M. Bice, A. Montanari, L. C. Cleaveland, K. T. Christianson, R. Coccioni, and L. A. Hinnov (2008), Oceanic anoxic cycles? Orbital prelude to the Bonarelli Level (OAE2), *Earth Planet. Sci. Lett.*, *267*, 1–16.

Monechi, S., and G. Parisi (1989), Da Gubbio a Cantiano, in *Stratigrafia del Mesozoico e Cenozoico nell'area umbro-marchigiana*, *Memorie Descrittive della Carta Geologica d'Italia*, vol. 39, edited by S. Cresta, S. Monechi, and G. Parisi, pp. 96–102, Istituto Poligrafico e Zecca dello Stato, Rome, Italy.
Mutterlose, J., A. Bornemann, and J. O. Herrle (2005), Mesozoic calcareous nannofossils—State of the art, *Palaontol. Z.*, *79*, 113–133.
Neuhuber, S., and M. Wagreich (2011), Geochemistry of Cretaceous oceanic red beds—A synthesis, *Sediment. Geol.*, *235*, 72–78.
Nowell, A. R. M., and C. D. Hollister (Eds.) (1985), *Deep Ocean Sediment Transport—Preliminary Results of the High Energy Benthic Boundary Layer Experiment*, Elsevier, New York.
Nowlin, W. D., Jr., and J. M. Hubert (1972), Contrasting summer circulation patterns for the eastern Gulf, in *Contributions on the Physical Oceanography of the Gulf of Mexico*, *Oceanographic Studies*, vol. 2, edited by L. R. A. Capurro and J. L. Reid, pp. 119–137, Gulf Publ. Co., Houston, Tex.
Pagani, M., M. Huber, and B. Sageman (2014), Greenhouse climates, in *Treatise on Geochemistry*, 2nd Ed., edited by H. D. Holland, and K. K. Turekian, pp. 281–304, Elsevier, Oxford, doi:10.1016/B978-0-08-095975-7.01314-0.
Pequegnat, W. E. (1972), A deep bottom current on the Mississipi Cone, in *Contributions on the Physical Oceanography of the Gulf of Mexico*, *Oceanogr. Studies*, vol. 2, edited by L. R. A. Capurro and J. L. Reid, pp. 65–87, Gulf Publ. Co., Houston, Tex.
Premoli Silva, I., E. Erba, and M. E. Tornaghi (1989), Paleoenvironmental signals and changes in surface fertility in Mid Cretaceous Corg-rich pelagic facies of the Fucoid Marls (central Italy), *Géobios Mémoire*, *11*, 225–236.
Premoli Silva, I., E. Erba, G. Salvini, D. Verga, and C. Locatelli (1999), Biotic changes in Cretaceous anoxic events, *J. Foram iniferal Res.*, *29*, 352–370.
Rebesco, M., and D. A. V. Stow (2001), Seismic expression of contourites and related deposits: A preface, *Mar. Geophys. Res.*, *22*, 303–308.
Robinson, S. R., L. J. Clarke, A. Nederbragt, and I. G. Wood (2008), Mid-Cretaceous oceanic anoxic events in the Pacific Ocean revealed by carbon-isotope stratigraphy of the Calera Limestone, California, *Geol. Soc. Am. Bull.*, *120*(11/12), 1416–1427.
Roth, P. H. (1978), Cretaceous nannoplankton biostratigraphy and oceanography of the northwestern Atlantic Ocean, in *Initial Reports of the Deep Sea Drilling Project*, vol. 44, edited by W. E. Benson et al., pp. 731–760, U.S. Gov. Print. Off., Washington, D. C.
Salmon, V., S. Derenne, E. Lallier-Vergés, C. Largeau, and B. Beaudoin (1998), Alteration of organic matter during chertification of a Cenomanian black shale (Umbria-Marche Basin, central Italy), *Mineral. Mag.*, *62A*(3), 1314–1315.
Schlanger, S. O., and H. C. Jenkyns (1976), Cretaceous oceanic anoxic events: Causes and consequence, *Geol. Mijnbouw*, *55*(3–4), 179–184.
Scholle, P. A., and M. A. Arthur (1980), Carbon isotope fluctuations in Cretaceous pelagic limestones: Potential stratigraphic and petroleum exploration tool, *AAPG Bull.*, *64*, 67–87.
Shanmugam, G. (2008), Deep water bottom currents and their deposits, in *Contourites*, *Dev. Sediment.*, vol. 60, edited by M. Rebesco and A. Camerlenghi, pp. 59–81, Elsevier, Amsterdam.
Shanmungam, G. (2006), *Deep-Water Processes and Facies Models: Implications for Sandstone Petroleum Reservoirs*, Elsevier, Amsterdam.
Sinnighe-Damsté, J. S., E. C. van Bentum, G.-J. Reichart, J. Pross, and S. Schouten (2010), A CO_2 decrease-driven cooling and increased latitudinal temperature gradient during the Mid-Cretaceous oceanic anoxic event 2, *Earth Planet. Sci. Lett.*, *293*, 97–103.
Sissingh, W. (1977), Biostratigraphy of Cretaceous calcareous nannoplankton, *Geol. Mijnbouw*, *56*, 37–65.
Skelton, P. W., R. A. Spicer, S. P. Kelley, and I. Gilmour (Eds.) (2003), *The Cretaceous World*, Cambridge Univ. Press, Cambridge, U. K.
Surlyk, F., and H. Lykke-Andersen (2007), Contourite drifts, moats and channels in the Upper Cretaceous chalk of the Danish Basin, *Sedimentology*, *54*, 405–422.
Tiraboschi, D., E. Erba, and H. C. Jenkyns (2009), Origin of rhythmic Albian black shales (Piobbico core, central Italy): Calcareous nannofossil quantitative and statistical analyses and paleoceanographic reconstructions, *Paleoceanography*, *24*, PA2222, doi:10.1029/2008PA001670.
Trabucho-Alexandre, J., E. Tuenter, G. A. Henstra, K. J. van der Zwan, R. S. W. van de Wal, H. A. Dijkstra, and P. L. de Boer (2010), The Mid-Cretaceous North Atlantic nutrient trap: Black shales and OAEs, *Paleoceanography*, *25*, PA4201, doi:10.1029/2010PA001925.
Tsikos, H., et al. (2004), Carbon-isotope stratigraphy recorded by the Cenomanian-Turonian oceanic anoxic event: Correlation and implications based on three key localities, *J. Geol. Soc., London*, *161*, 711–719.
Turgeon, S. C., and R. A. Creaser (2008), Cretaceous oceanic anoxic event 2 triggered by a massive magmatic episode, *Nature*, *454*, 323–326.
Turgeon, S., and H.-J. Brumsack (2006), Anoxic vs dysoxic events reflected in sediment geochemistry during the Cenomanian–Turonian boundary event (Cretaceous) in the Umbria–Marche Basin of central Italy, *Chem. Geol.*, *234*, 321–339.
van Helmond, N. A. G. M., et al. (2016), Equatorward phytoplankton migration during a cold spell within the Late Cretaceous supergreenhouse, *Biogeosci. Discuss.*, doi:10.5194/bg-2015-659.
Voigt, S. (2008), Saline water sinking, *Nat. Geosci.*, *1*, 423–424.
Voigt, S., A. S. Gale, and T. Voigt (2006), Sea-level change, carbon cycling and palaeoclimate during the Late Cenomanian of northwest Europe: An integrated palaeoenvironmental analysis, *Cretaceous Res.*, *27*, 836–858.
Voigt, S., A. Aurag, F. Leis, and U. Kaplan (2007), Late Cenomanian to Middle Turonian high-resolution carbon isotope stratigraphy: New data from the Münsterland Cretaceous Basin, Germany, *Earth Planet. Sci. Lett.*, *253*, 196–210.
Volpi, V., A. Camerlenghi, C.-D. Hillebrand, M. Rebesco, and R. Ivaldi (2003), The effect of biogenic silica on sediment consolidation and slope instability, Pacific margin of the Antarctic Peninsula, *Basin Res.*, *15*, 339–354.
Wang, C., X. Hu, Y. Huang, M. Wagreich, R. Scott, and W. Hay (2011), Cretaceous oceanic red beds as possible consequence of oceanic anoxic events, *Sediment. Geol.*, *235*, 27–37.
Weissert, H., J. A. McKenzie, and J. E. T. Channell (1985), Natural variations in the carbon cycle during the Early Cretaceous, in *The Carbon Cycle and Atmospheric CO_2: Natural Variations Archean to Present*, *Geophys. Monogr. Ser.*, vol. 32, edited by E. T. Sundquist and W. S. Broecker, pp. 531–545, AGU, Washington, D. C.
Weissert, H., A. Lini, K. B. Föllmi, and O. Kuhn (1998), Correlation of Early Cretaceous carbon isotope stratigraphy and platform drowning events: A possible link?, *Palaeogeogr. Palaeoclimatol. Palaeoecol.*, *137*, 189–203.
Wilson, P. A., and R. D. Norris (2001), Warm tropical ocean surface and global anoxia during the Mid-Cretaceous period, *Nature*, *412*, 425–429.
Winterer, E. L., and A. Bosellini (1981), Subsidence and sedimentation on a Jurassic passive continental margin (Southern Alps, Italy), *AAPG Bull.*, *65*, 394–421.
Wohlwend, S., M. Hart, and H. Weissert (2015), Ocean current intensification during the Cretaceous oceanic anoxic event 2—Evidence from the northern Tethys, *Terra Nova*, *27*, 147–155, doi:10.1111/ter.12142.
Xi, C., C. Wang, X. Hu, Y. Huang, P. Wang, L. Jansa, and X. Zeng (2007), Cretaceous oceanic red beds: Distribution, lithostratigraphy and paleoenvironments, *Acta Geologica Sinica*, *81*, 1070–1086.
Young, J. R. (1994), Functions of coccoliths, in *Coccolithophores*, edited by A. Winter and W. G. Siesser, pp. 63–82, Cambridge Univ. Press, Cambridge.
Zheng, X., H. C. Jenkyns, A. S. Gale, D. J. Ward, and G. M. Henderson (2016), A climatic control on reorganization of ocean circulation during the mid-Cenomanian event and Cenomanian-Turonian oceanic anoxic event (OAE 2): Nd isotope evidence, *Geology*, *44*, 151–154.